Noise-assisted persistence and recovery of memory state in a memristive spiking neuromorphic network

I.A. Surazhevsky[1], V.A. Demin[1], A.I. Ilyasov[1,2], A.V. Emelyanov[1,3], K.E. Nikiruy[1], V.V. Rylkov[1,4], S.A. Shchanikov[5,6], I.A. Bordanov[5], S.A. Gerasimova[6], D.V. Guseinov[6], N.V. Malekhonova[6], D.A. Pavlov[6], A.I. Belov[6], A.N. Mikhaylov[6], V.B. Kazantsev[6], D. Valenti[6,7], B. Spagnolo[6,7,8], M.V. Kovalchuk[1,2]

[1] National Research Center "Kurchatov Institute", 123182 Moscow, Russia

[2] Faculty of Physics, Lomonosov Moscow State University, 119991 Moscow, Russia

[3] Moscow Institute of Physics and Technology (State University), 141700 Dolgoprudny, Moscow Region, Russia

[4] Kotelnikov Institute of Radio Engineering and Electronics RAS, 141190 Fryazino, Moscow Region, Russia

[5] Department of Information Technologies, Vladimir State University, 600000 Vladimir, Russia

[6] Lobachevsky University, 603950 Nizhny Novgorod, Russia

[7] Dipartimento di Fisica e Chimica-Emilio Segrè, Group of Interdisciplinary Theoretical Physics, Università di Palermo, Viale delle Scienze, Edificio 18, I-90128 Palermo, Italy

[8] Istituto Nazionale di Fisica Nucleare, Sezione di Catania, Via S. Sofia 64, 95123 Catania, Italy

Abstract

We investigate the constructive role of an external noise signal, in the form of a low-rate Poisson sequence of pulses supplied to all inputs of a spiking neural network, consisting in maintaining for a long time or even recovering a memory trace (engram) of the image without its direct renewal (or rewriting). In particular, this unique dynamic property is demonstrated in a single-layer spiking neural network consisting of simple integrate-and-fire neurons and memristive synaptic weights. This is carried out by preserving and even fine-tuning the conductance values of memristors in terms of dynamic plasticity, specifically spike-timing-dependent plasticity-type, driven by overlapping pre- and postsynaptic voltage spikes. It has been shown that the weights can be to a certain extent unreliable, due to such characteristics as the limited retention time of resistive state or the variation of switching voltages. Such a *noise-assisted persistence of memory*, on one hand, could be a prototypical mechanism in a biological nervous system and, on the other hand, brings one step closer to the possibility of building reliable spiking neural networks composed of unreliable analog elements.

Introduction

Although CMOS-based traditional hardware with the Von-Neumann architecture has achieved significant advances in computing, it may not be optimal for emerging tasks of machine learning and artificial neural networks [1-2]. In this respect, neuromorphic (bio-inspired) computing based on memristive devices may offer dramatic performance improvements in solving computationally hard problems [3-4]. Indeed, memristive devices, although the diffusion, stability, and switching mechanisms are not yet fully understood [5-9], remain excellent promising candidates for neuromorphic computing [10-11]. Actually, the promising neuromorphic computing circuits based on memristive weights, such as perceptrons [12-17], long short-term memory [18], reservoir computing [19], Hopfield network [20] and others [21] have been demonstrated. However, learning in these formal neuromorphic networks requires additional computing blocks for calculating error (or loss function) gradients and accurate updates of the weights with a need for their implementation in hardware which suffers from memristor variability issue [22]. On the contrary, in spiking neuromorphic networks (SNNs) it is possible to realize at least partially unsupervised learning in terms of a spike-timing-dependent plasticity (STDP) mechanism [23-28]. The STDP was shown to emerge naturally in different memristive devices [29-34]. Moreover, the STDP-based learning of SNN provides self-adaptation of the memristor resistive states and makes the plasticity sensitive only to the input signal configuration, but neither to the initial state of the devices nor to their device-to-device variability [35]. Despite their high potential, the computational capability of SNNs has not been widely demonstrated in comparison with formal architectures, mainly because of the lack of efficient learning algorithms [36]. Therein, different stochastic and noise effects [17,37-39] may offer new insights into the problem.

When dealing with SNNs, especially biological ones, noise is generally its inherent property. It comes from input spike sequence usually obeying Poisson-like distribution, from synaptic weight fluctuations [40], from partially random character of ion channel operation [41], from random fluctuations of ion and neurotransmitter concentrations outside of a neural cell [42], and from other sources of stochasticity. Recent investigations have shown the constructive role of noise in nonlinear systems far from equilibrium [43-53]. Indeed, noise plays a crucial role in several well-established phenomena such as stochastic resonance [54-58], noise enhanced stability [59-64], and stochastic resonant activation [65-67]. Furthermore, a coherent response in neuronal systems was observed, such as stochastic resonance in neurons [68], noise focusing [69], transient recovery mechanism [70], and synchronization phenomena. Noise is often useful for learning algorithms of formal ANNs [71]. Recently, in the SNN with

STDP-like weight update simulation of a culture composed of cortical-like neuron cells it was shown that noise can enhance the structural changes in the network with the formation of synaptic couplings of neurons in a region with applied external stimulus [72]. This could lead to faster learning of the network. Also the coupling of two cortical neurons in brain slices via organic memristive devices was demonstrated to support synchronized delta- oscillations [73]. Nevertheless, to the best of our knowledge, there were no physical or simulation experimental demonstrations of possible constructive role of input noise in memristive SNN learning and persistent storage of memorized patterns. At the same time, this issue is of high significance due to variability and reliability problems in arrays of non-ideal analogue elements such as memristors.

In this paper, we raise the question of whether it is possible to maintain the set values of the synaptic weights, in the process of pre-training, of a single-layer SNN by supplying all its inputs with a low-rate noise signal with the same average pulse frequency. This signal obviously does not encode any useful pattern, so we will refer to it as the noise pattern, or simply the noise. The given question is particularly important in light of different sources of real memristive device non-idealities such as the finite retention times of resistive states, the variability of switching voltages both from device-to-device and cycle-to-cycle points of view, and others [74-76]. The proposed yet energy-efficient approach is to try to overcome various imperfections of analogue memristive devices by simply applying a low-frequency noise pattern to the SNN inputs. This could allow maintaining some memorized data stored in the memristive weights, or even allow their refreshing driven by the applied noise.

The idea of holding weights by a low-rate signal at the inputs is based mainly on the occurrence of a stable fixed postsynaptic neuron frequency because of weight-dependent correlation between pre- and postsynaptic low-rate signals in the case of pair-based additive STDP [77]. Briefly, Sboev et al. have shown that at some ranges of parameters, some number of inputs with large synaptic weights together drive the postsynaptic neuron activity and simultaneously break the possibility of growing low weights, in terms of additive STDP updates (see also the Discussion section).

Although memristive STDP may differ significantly from the simplest theoretical additive mechanism of dynamic plasticity, this hypothesis is quite universal from theoretical point of view and useful in applied sense to deserve an experimental verification. At the same time, some similar mechanism may have place in the reliable persistence of memory in a biological nervous system built from a large number of unreliable elements (see also the Discussion section for more details).

Here, we demonstrate the possibility of *noise-assisted learning* of SNNs based on two types of memristors: nanocomposite $(CoFeB)_x(LiNbO_3)_{100-x}$ (CFB-LNO NC) [78] and $ZrO_2(Y)$-based [79] devices. The possibility of weight update according to STDP type of Hebbian law, as the basic condition for SNN training, is demonstrated for both CFB-LNO NC and $ZrO_2(Y)$-based memristors. The capability of re-learning after switching high rate inputs to low rate and vice versa with different presynaptic spike frequency ratio is also shown in the physical experiment for CFB-LNO NC memristors.

Thereafter, based on different model behavior of CFB-LNO NC and $ZrO_2(Y)$-based memristors, computer simulation of the influence of memristor nonidealities such as limited retention times and switching voltage variability on the *noise-assisted learning* is thoroughly investigated. The possible reasons and interesting consequences of such unique dynamic system properties are considered in the Discussion section and inferred in Conclusions.

Materials and Methods

To show some universality of the proposed approach, two types of memristive device structures are used in this work. The first one is based on CFB-LNO NC ~1μm-width layer with a thin (~20 nm) interlayer of amorphous $LiNbO_3$ (Fig. 1a). The CFB-LNO NC layer consists of CoFe nanogranules of 2-3 nm size in $LiNbO_3$ matrix [78]. The electroforming-free memristive structures were made in the standard metal/NC/metal geometry, and NC layer was deposited by ion-beam sputtering of a composite target in an argon atmosphere ($P_{Ar} = 5.6 \cdot 10^{-4}$ Torr). The top and bottom electrodes were Cr/Cu/Cr films with the top electrode size of 0.5x0.2 mm^2 (for details see Ref. [78]).

The second type of studied memristive structures is based on yttria-stabilized zirconia ($ZrO_2(Y)$) as a switching material superior in terms of oxygen vacancy content well controlled by doping and high mobility of oxygen ions due to a low activation energy of 0.5-0.7 eV [80-82]. Industrial bi-layer TiN/Ti metallization deposited on the oxidized SiO_2/Si substrate by magnetron sputtering of Ti target was used as bottom electrode. The $ZrO_2(Y)$ film with a thickness of around 40 nm was deposited by RF-magnetron sputtering of ZrO_2 (12 mol.% Y_2O_3) target using the 2G1-1G2-EB4-TH1 setup (Torr International) in the argon-oxygen gas mixture (50% oxygen content) at the pressure of 1.8×10^{-2} Torr and substrate temperature of 300°C. Top Au electrode with a thickness of 40 nm and a thin Zr adhesion sublayer (3 nm) was deposited by the method of DC-magnetron sputtering in an argon atmosphere at the pressure of 5×10^{-3} Torr and substrate temperature of 200°C.

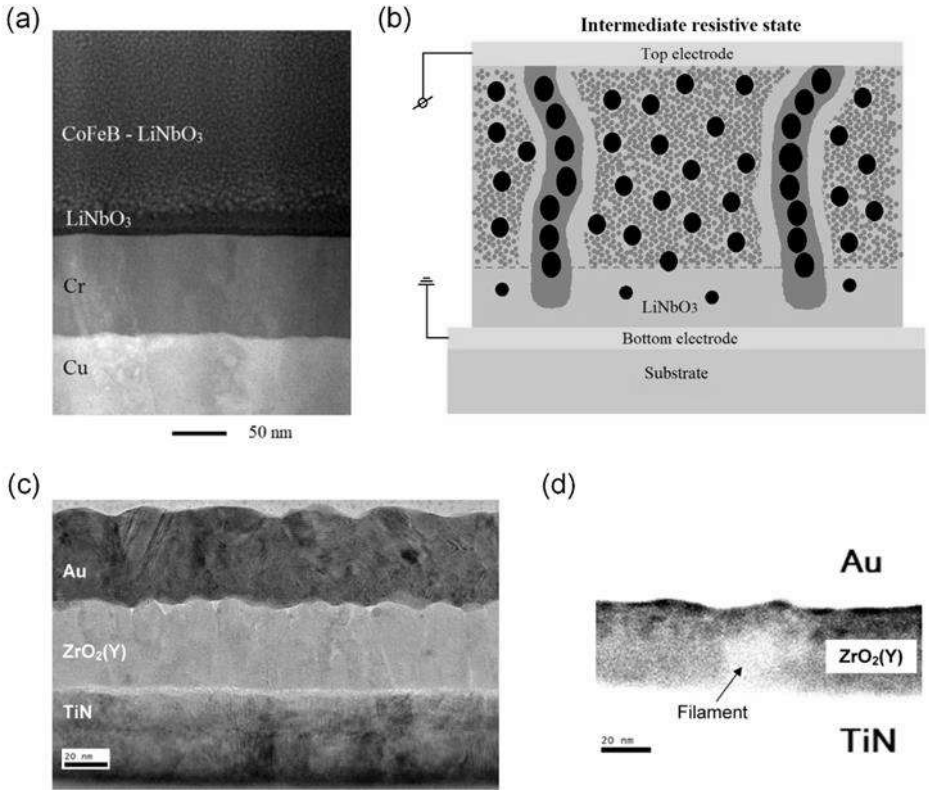

Fig. 1. (a) Dark-field scanning transmission electron microscopy images of the $M/(CoFeB)_x(LiNbO_3)_{100-x}/M$ structure near the bottom electrode. (b) Structure scheme explaining the mechanism of resistive switching. Green color shows an amorphous $LiNbO_3$ matrix containing metal CoFe nanograins (black ovals) and a nonequilibrium phase of Co and Fe atoms with a concentration reaching ~ 10^{22} cm^{-3} (grey dots). Green dashed line separates the high-resistance layer near the bottom electrode of the structure from the predominantly stoichiometric $LiNbO_3$, in which there is no a non-equilibrium atomic metallic phase. Grey areas surrounding the chains of granules represent a metal condensate, which arises due to the processes of nucleation of Co and Fe atoms and oxygen vacancies when current flows through the structure. (c) Cross-sectional high resolution transmission electron microscopy (HRTEM) image of the pristine Au/Zr/ZrO_2(Y)/TiN/Ti memristive structure and (d) cross-sectional dark-field STEM image showing the filament area in the ZrO_2(Y) film after electroforming.

The microscopic cross-sectional images of CFB-LNO NC and ZrO_2(Y)-based memristive structures were studied by the methods of scanning transmission electron microscopy (STEM) and high-resolution transmission electron microscopy (HRTEM), respectively, on the basis of Titan 80-300 and JEM-2100F (JEOL) systems. The STEM scans for ZrO_2(Y)-based samples were analyzed before and after electroforming to look for images with the filament areas emerged (Fig. 1d). The cross sections of memristive devices were prepared by conventional technology using the equipment of Gatan Inc.

The *I-V* curves and STDP windows were obtained using 4-channel SMU NI PXIe-4140. Current limits of +50 mA (for CFB-LNO NC) and -200 μA (for ZrO_2(Y)) were used while

obtaining *I-V* curves to prevent memristors from breakdown in the range where the switching to the low resistance state occurs (positive voltage on top electrode for CFB-LNO NC and negative for ZrO_2(Y)-based structure).

In STDP measurements, two software neurons were emulated, time difference between their spikes is represented as Δt coordinate ($\Delta t = t_{post} - t_{pre}$). Each point of STDP window curve was measured as follows: first, a memristor was switched to pre-determined initial resistance state using specially designed algorithm [83], then a pair of impulses of pre- and postsynaptic events with given time difference was applied to memristor, and after that, its final conductance was measured and plotted as the difference $\Delta G = \left(G_{final} - G_{initial}\right)/G_{initial}$ vs. Δt. Each point of an STDP curve is the result of averaging over ten repetitions.

In the Hebbian learning physical experiments, four software presynaptic neurons (just playing the role of pulse generators) are connected via four memristors to one specially designed integrate-and-fire hardware postsynaptic neuron, see Fig. 5a and Ref. [84] for details. During a 1-second-long learning cycle each pre-neuron produces pulses with a given shape and at a given rate (1 - 10 Hz). Timing of these pulses is random, in accordance with Poisson distribution. Pre-spikes from each presynaptic neuron are applied to bottom electrode of corresponding memristor and, being weighted through it, charge the capacitor of post-neuron, increasing its membrane potential. When this potential exceeds a certain threshold value, post-neuron generates spike which is applied to the top electrodes of all four memristors, driving their update through overlapping with pre-spikes. After each learning cycle, memristor conductances are consecutively measured by source measurement unit (SMU) [85], and no pre- or post-spikes are generated during this process. Both pre- and postsynaptic spikes were chosen sawtooth shaped, with the following parameters (amplitude and duration) of their left and right shoulders: (a) for CFB-LNO NC, pre-spike, +6V (45ms), -5V (35ms), and post-spike, +4.8V (32ms), -5.8V (50ms); (b) for ZrO_2(Y)-based device, pre-spike, +4.2V (31ms), -4.1V (24ms), and post-spike, +3.8V (27ms), -4.4V (33ms). These parameters were chosen to provide a small decrease of a memristor conductivity by each of presynaptic spike for most of the memristive devices. This is necessary for correct Hebbian separation of synaptic weights at different rates of pulses at inputs.

In computer simulation, different memristor models are used to simulate their electrical characteristics. In the case of CFB-LNO NC memristive device, the voltage ThrEshold adaptive memristor (VTEAM) model is exploited for the conductivity G and a synaptic weight $w = (G - G_{min})/(G_{max} - G_{min})$ for modeling the behavior of the device [86]. Its advantages are the presence of a quite large number of configurable parameters connected to real empirical

properties of memristor, that is resistances in high and low resistive states, threshold switching voltages, rate constants of an internal state variable responsible for the speed of resistive switching, window functions for setting behavior of an internal variable at its bounds. In addition to the functionality described, resistance relaxation process to some pre-determined final resistive state due to a finite retention time was programmed to perform this study.

To describe the realistic CFB-LNO NC device dynamic and overall behavior, the memristor model was tuned by approximating its experimental *I-V* characteristics (Fig. 2a,c). VTEAM parameters were set by the following values: resistance of the low-resistance state R_{on} = 1 kOhm, resistance of the high-resistance state R_{off} = 30 kOhm, switching voltage for the SET mode, V_+ = 3 V, and RESET mode, V_- = -3 V. The final stable resistive state of the memristor was randomly defined from a normal distribution which was based on experimental retention time measurement data. As for neurons, the previously developed Verilog-a model with adjustable parameters was exploited in Ref. [87]. The model parameters were set to values +2 V (40 ms), -2.5 V (20 ms), and +2 V (30 ms), -4.5 V (30 ms) for amplitude and duration of pre- and postsynaptic bi-triangular spikes, respectively.

In the case of ZrO_2(Y)-based memristors, simulations were performed in custom-made Python framework with the use of implemented previously integrate-and-fire models of neurons [87] and a specialized memristor model [88] as a synaptic weight, which is also calibrated to the experimental data, see Fig. 2b,d. The model itself has 7 configurable parameters. Among them are the activation energies for ion migration and electron transport in the high-resistance state, so that the model *I-V* curve quite accurately describes the switching dynamics of real ZrO_2(Y)-based samples. It should be noted that it does not support the retention time parameter setting because of its high value for all ZrO_2(Y)-based samples ($> 10^4$ s), and since the dynamics of samples is determined mostly by the activation energy of ions and the cycle-to-cycle variability of switching voltages.

To demonstrate the possibility of noise-assistant training, a circuit of four presynaptic neurons and one postsynaptic neuron, see Fig. 5a, was implemented using memristor models described above. On this basis, several series of experiments were carried out. For CFB-LNO NC memristors, they are characterized by the following setup configurations: i) the voltage variation is absent (equals to 0%), while the retention time is varied: 10^2 s, 10^3 s, and 10^5 s (the last one is considered as infinite retention time); ii) the retention time remains unchanged and equals to 10^3 s, while the relative standard deviation of both switching voltages is set at 5%, 10%, 15%, or 25%. The specific voltages are chosen from normal distribution for each memristive weight and remain fixed at further simulation. This corresponds to device-to-device variability.

Each series of simulation experiments with CFB-LNO NC memristors consists of 3 stages:

1. Hebbian postsynaptic neuron learning with 1-1-10-10 Hz input rates ('Hebb' stage);
2. Noise-assisted update of synaptic weights with 1Hz Poisson trains of pulses at all inputs ('Noise' stage);
3. Relaxation process of weights with disabled input spike generator ('Free' stage).

To collect statistics, each experiment is performed 10 times.

For ZrO_2(Y)-based devices, only 2 stages of simulation learning were conducted, namely 'Hebb' and 'Noise' stages, since the retention time is infinite for these samples, and 'Free' stage can be eliminated. In this case, the training simulation is done with variations in activation energy, cycle-to-cycle change in switching voltages and memristor conductance in a high-resistance state. Each simulation is repeated 10 times.

Results

I-V and STDP measurements

Typical *I-V*-curves of our memristors are presented in Fig. 2. CFB-LNO NC-based structures demonstrate fairly good memristive characteristics (Fig. 2a): endurance is not less than 10^6 switching cycles [35], retention time (but not for all samples) > 10^5 s [84], multilevel switching > 256 resistive states [89], and high switching rate < 10 ns [56]. This is likely due to the high content of dispersed Co and Fe atoms in the insulating $LiNbO_{3-y}$ matrix (up to ~10^{22} cm^{-3} [79, 91]) and the presence near a bottom electrode of the high-resistance amorphous $LiNbO_3$ interlayer (about 10 nm) with permittivity ε_d reaching ~ (10^2–10^4). Fig. 1b schematically illustrates the qualitative resistive switching model in CFB-LNO NC memristive structures. In a pristine state the dispersed atoms are uniformly distributed in the isolating matrix. At the first switching cycle at a positive voltage, nucleation of dispersed atoms around chains of nanogranules occurs. This produces percolation paths, which form the metalized granular chains almost, but not totally, connecting the top and bottom electrodes (in the $LiNbO_3$ interlayer the migration of oxygen vacancies is probably dominating) [79, 92]. Herewith, the structure switches to the low resistive state without the need for voltages higher than at the following cycles, that is it has electroforming-free behavior. When a sufficiently large negative voltage is applied to the top electrode, the structure switches back to the high (or intermediate) resistive state due to the movement of oxygen vacancies toward the top electrode likely alongside the metalized granular chains that increase the effective gap between the chains and the bottom electrode (see Fig. 1b). It is crucial that the number of the metalized granular chains in CFB-LNO NC structures is rather high (10^{10}-10^{11} cm^{-2}) [79], what could be the reason for the good memristive characteristics mentioned above and appropriate for neuromorphic

applications. Figure 1c shows an HRTEM image of the Au/Zr/ZrO_2(Y)/TiN/Ti memristive structure cross section. The ZrO_2(Y) film is located between the conducting electrodes of Au and TiN and reveals a columnar polycrystalline structure with a typical grain size about 10 nm and a high density of grain boundaries (10^{11}–10^{12} cm^{-2}). It is worth noting that the electrode/oxide interfaces are not flat, and the roughness generally correlates with the grain boundaries. After electroforming at negative bias and first switching cycles, a redistribution of oxygen in the film and a certain improvement of the contrast of the grain boundaries are observed [93]. Important information is obtained for the structure subjected to electroforming by scanning transmission electron microscopy (STEM) in the dark field mode, in which the contrast depends on the atomic number and concentration of chemical elements localized in the area of analysis. In particular, bright contrast at the top and bottom of the image in Fig. 1d corresponds to the layers containing Au and Ti heavy metals, respectively.

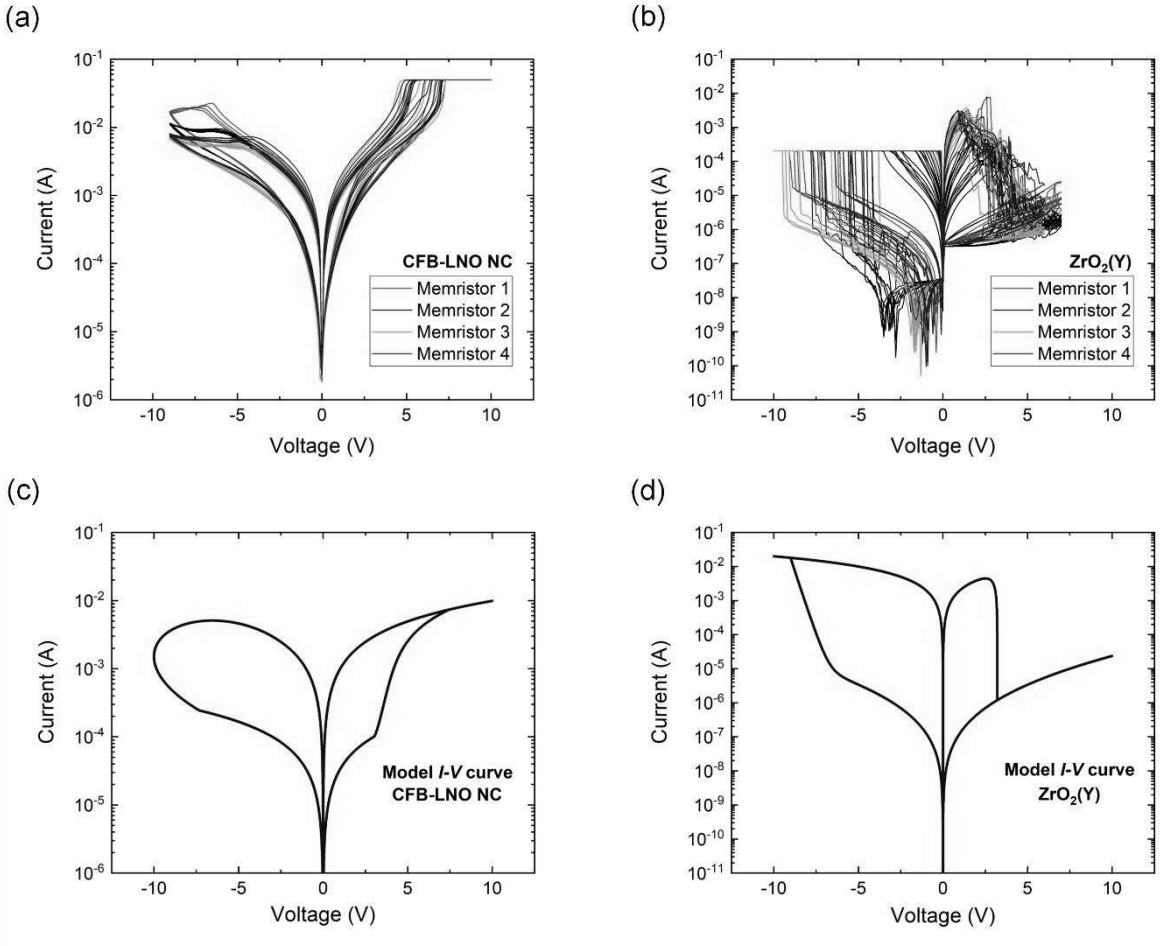

Fig. 2. Cyclic current-voltage (*I-V*) characteristics, measured for (a) CFB-LNO NC memristors, at 2 V/s scanning speed and 0.1 V resolution; (b) ZrO_2(Y)-based memristors, in voltage scanning mode with 2 V/s speed and 0.1 V resolution. Insets show model *I-V* curves for the corresponding memristive structures; (c) simulated *I-V* curve for CFB-LNO NC memristor; (d) simulated *I-V* curve for ZrO_2(Y)-based memristor.

The Z-contrast features associated with the changes in composition of oxide film and/or the density of material during electroforming are observed in the center of the ZrO_2(Y) layer. Such areas are absent in the samples before electroforming and are probably related to the formation of conductive filaments responsible for resistive switching. The ZrO_2(Y)-based memristive structure demonstrates bipolar resistive switching (Fig. 2b) of anionic type (valence-change mechanism) originated from the recovery and oxidation of conductive filaments [94]. Typical memristive characteristics achieved for this type of devices [80, 94] include the endurance > 10^5 switching cycles, retention time > 10^4 s and high switching speed (switching time as low as 50 ns). The devices show reproducible resistive switching with certain cycle-to-cycle and device-to-device variation of resistive states and switching voltages (see Fig. 2b) used to calibrate the parameters of corresponding dynamical model presented below.

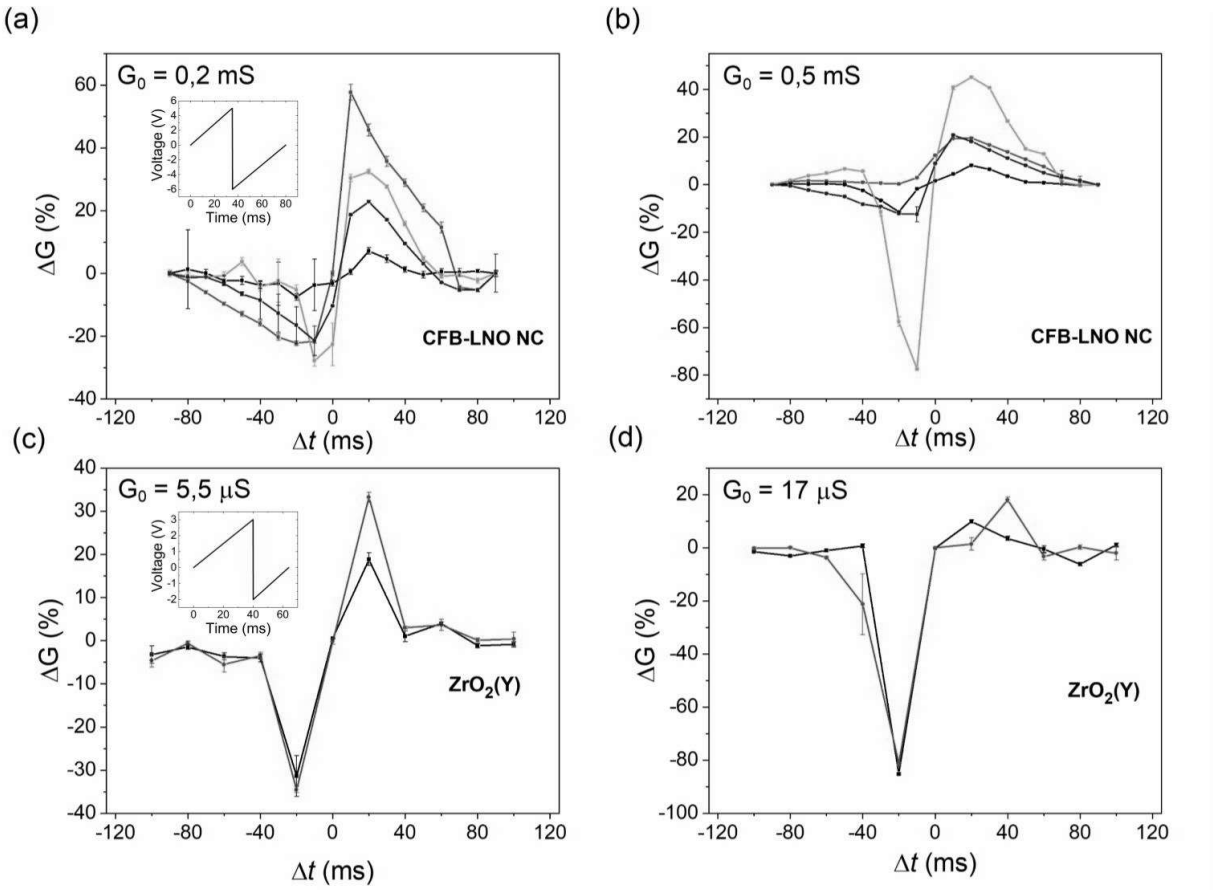

Fig.3. (a), (b) STDP windows for the 4 CFB-LNO NC memristors starting from the different initial conductivity states G_0. Pre- and postsynaptic spikes were identical, with a bi-triangular shape (inset in plot (a)) and the following parameters: +5 V positive shoulder amplitude and 35 ms duration, -6 V negative shoulder amplitude and 45 ms duration. (c), (d) STDP curves for the two ZrO_2(Y)-based memristors, with also identical bi-triangular shape pre- and post-spikes (inset in plot (c)) having the following parameters: +3 V and 40 ms, and -2 V and 24 ms, for the positive and negative shoulders of the spike, respectively.

All the STDP windows, for both types of memristors and all initial conductance states (Fig. 3), show increase of conductivity when time difference Δt between post- and presynaptic spikes is small and positive, so that post-spike comes just after pre-spike and, therefore, correct cause-effect relationship between them is observed. Oppositely, the conductivity decrease takes place when pre-spike is fired after post-spike that manifests itself by wrong causal relationship. When comparing the STDP windows obtained for the same memristor type but different initial conductances (Fig.3 a-b and c-d), the following standard multiplicative-like regularity can be noted: the more initial conductance of memristor is, the less it increases and more decreases at any delay Δt.

Hebbian learning in physical experiments

The results of Hebbian learning experiments with 10-to-the-1 (10 : 1) presynaptic spike rate ratio are shown in Fig. 4 for both types of memristive devices (see also Fig. S1 for 10 : 2 and 10 : 5 ratio results for the case of CFB-LNO NC memristors). In Fig. 4a is shown the dependence of CFB-LNO NC conductivity on total learning time. During the first 400 seconds memristors 1 (red) and 2 (green) get the high presynaptic spike rate, and their conductivities increase becoming significantly higher than conductivities of memristors 3 (black) and 4 (blue).

After that, the rates of presynaptic spikes were reversed, so the first and the second pair of pre-neurons started to generate pulses with 1 Hz and 10 Hz rates, respectively. Again, high frequency inputs drive the increase in conductance of corresponding memristors. This is due to above-mentioned cause-effect temporal structure of the STDP window's positive part. When high-rate inputs activate the post-neuron firing more frequently than the low-rate ones, this causes the positive updates of the corresponding memristor conductivities. At the same time, the negative part of the STDP window, along with the mentioned preset inhibiting influence of separate presynaptic spikes, provides the decrease of memristor conductivities with the low-rate drive at their input.

Fig. 4b shows only the first stage of Hebbian learning (that is without further re-training) for ZrO_2(Y)-based memristors that results in conductance differentiation of memristors with low and high input rates after some period of stochastic switches between boundary memristive states. It can be noted that transition between different resistive states in CFB-LNO NC memristors occurs more gradually, via many intermediate states, while ZrO_2(Y)-based devices demonstrate much faster and abrupt switching. The reason for this is likely the quite high switching voltage cycle variability for the ZrO_2(Y)-based structure and its rich internal stochastic dynamics of filament edge formation and disruption. This may also be the reason

why it is much harder to obtain stable Hebbian learning with the latter type of memristive devices.

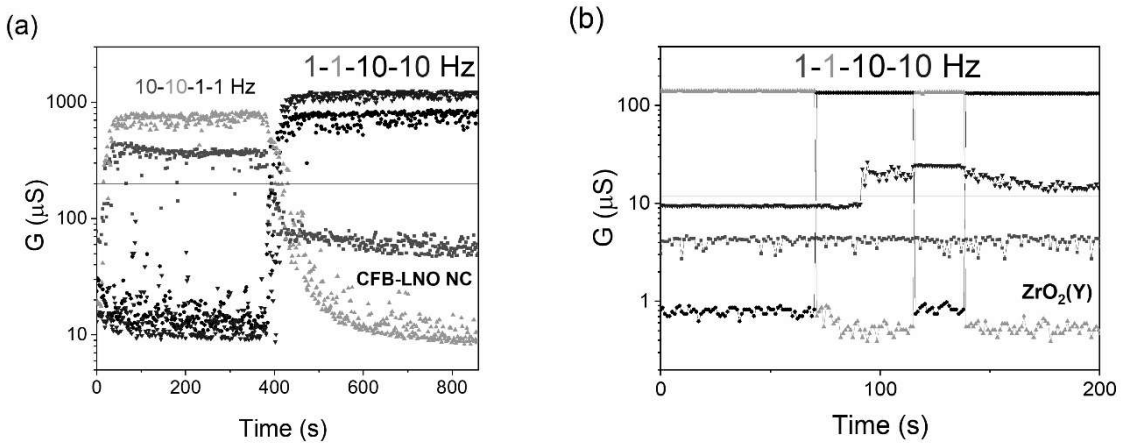

Fig. 4. Temporal trace of conductivity that shows experimental Hebbian learning in 4-to-1 SNN with (a) CFB-LNO NC and (b) ZrO_2-based memristors. Both plots represent similar pre-spike rate ratio at the inputs: 10 Hz : 1 Hz. Impulse parameters: a) pre-spikes +6 V (45 ms), -5 V (35 ms); post-spikes +4.8 V (32 ms), -5.8 V (50 ms); (b) pre- and postsynaptic spikes are identical: +3 V (40 ms), -2 V (24 ms). Each point shows conductivity of memristor after one learning cycle with 1 second-long duration. Demarcation lines (in grey) are just guides for the eye.

It should be noted that both memristive structures fail to provide experimentally the preservation of memristor conductivities under Poisson-distributed pulse trains with the same low rate applied to all inputs (i.e. at the noise input). Preliminary analysis hints that this is probably due to nonideal characteristics of the devices. CFB-LNO NC memristors possess insufficiently long durations of storing the resistive states (retention times), whereas ZrO_2(Y)-based structures suffer from high cycle-to-cycle and device-to-device switching voltage variation. This assumption inspired us to conduct the simulation experiments at which different ranges of characteristics of plausible memristor-specific models could be tested.

Hebbian and noise-assisted learning in simulation experiments

The results of the first series of experiments on noise-assisted training for CFB-LNO NC using the scheme described in the 'Samples and Methods' section are shown in Fig. 5. In particular it is shown, in Fig. 5a the schematic representation of the 4-to-1 SNN, and in Fig. 5b-5d the dynamics of four synaptic weights. Highlighted in bold trends are the average behaviors calaculated on 10 experimental runs each. The Hebbian learning stage occurs in the first 50 seconds with time distributed Poisson pulse trains of different average frequencies at different inputs: 1Hz for W1 and W2, 10Hz for W3 and W4. Then afterwards, the noise signal at the

average frequency of 1Hz is applied to all inputs during 200 s in (c), (d), and 950 s in (b). Finally, the free relaxation process of resistive states, without any signal on the inputs, is shown during the last 50 seconds in plots (c) and (d). In plot (b) the relaxation process (Rel 1-4 curves) is shown alongside with noise-assisted training stage, in order to make a clear difference between maintaining, or even slightly consolidating, the memory trace, encoded in array of memristive weights, and its eruption due to "forgetting" the synaptic efficacies. From Fig. 5c we see that, according to our assumption, low retention time of memristors does not allow to preserve their resistive states achieved during pattern-specific Hebbian training of the 4-to-1 SNN (Fig. 5a), by application of the low-rate Poisson train to all 4 inputs (noise signal).

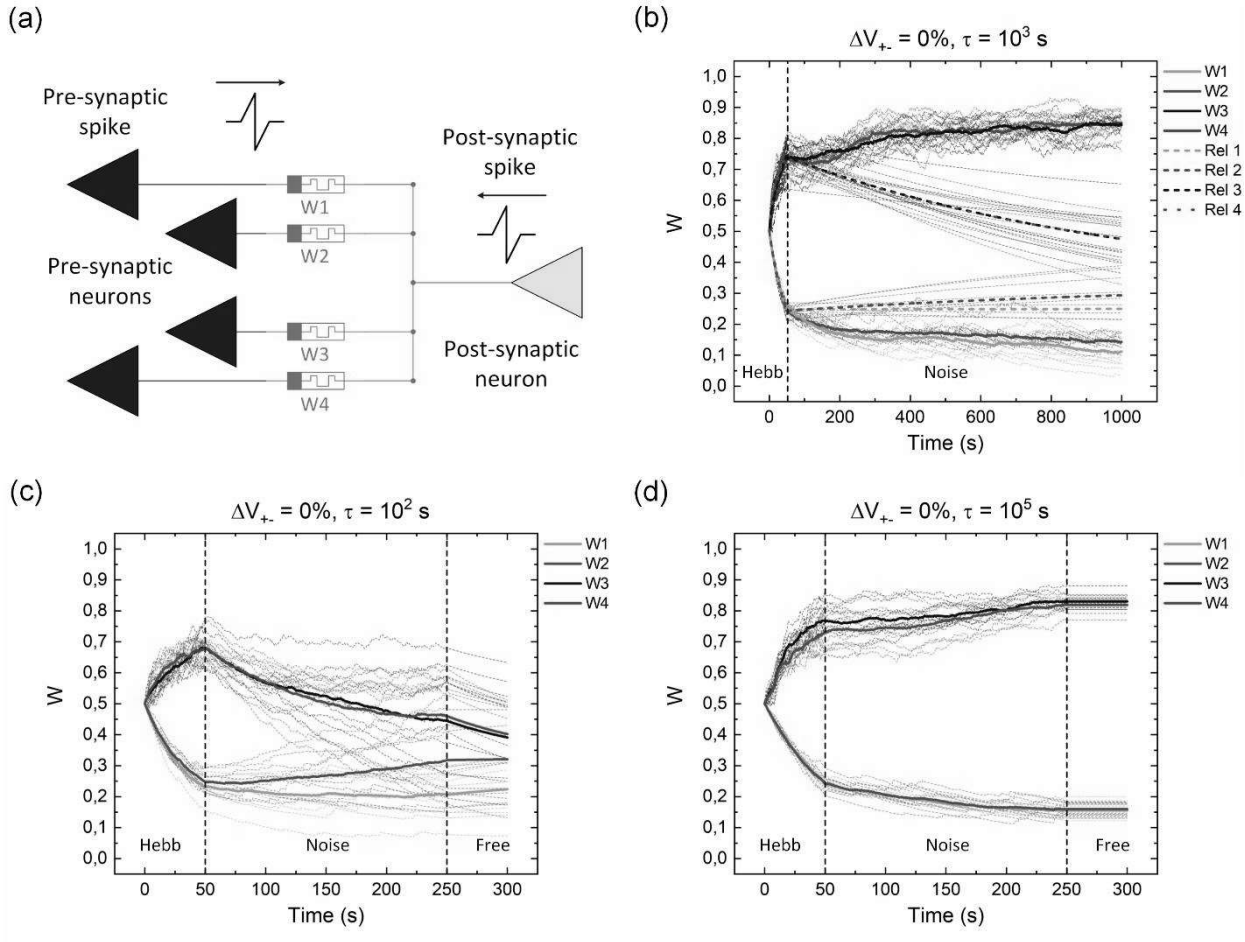

Fig. 5. (a) Schematic representation of the 4-to-1 SNN. (b)-(d) Temporal behaviors of conductivity in the SNN simulation with different retention times: (b) 10^3 s; (c) 10^2 s; (d) 10^5 s; at a constant memristor switching voltages ($\Delta V_{+-} = 0$ %), with highlighted in bold trends the average behaviors calaculated on 10 experimental runs each. Hebbian learning stage in the first 50 seconds with time distributed Poisson pulse trains of different average frequencies at different inputs: 1Hz for W1 and W2, 10Hz for W3 and W4. Then, the noise signal at the average frequency of 1Hz is applied to all inputs during 200 s in (c), (d), and 950 s in (b). The free relaxation process of resistive states, without any signal on the inputs, is shown during last 50 seconds in plots (c), (d), and (b) with the curves Rel 1-4 curves.

By increasing the retention time up to 10^3 seconds, the input noise signal allow not only to hold resistive states, but also to continue the learning process, i.e. consolidating a memory trace, or engram, about learned pattern (Fig. 5b). This prevents the weights from sliding into some fixed but randomly chosen for each memristor final stable states, as it can be evident from comparison of the *noise-assisted learning* curves with relaxation process captured by Rel 1-4 temporal dependencies, for which no any signal is applied to the inputs. The same is true for greater retention time values (Fig. 5d).

The second series of experiments with CFB-LNO NC, shown in Fig. S2, was aimed at analyzing the influence of memristor switching voltages variation at a constant retention time of 10^3 seconds on the process of *noise-assisted learning*. An important point in its implementation is the pre-trained state of memristors, achieved at the end of Hebbian learning stage, just before the noise signal application to the network. The duration of the Hebbian training of 50 seconds, as it was in the previous series (Fig. 5), is insufficient to achieve acceptable results with a variable switching voltage, since the weights do not have time to disperse enough (Fig. S2 in Supplementary Material), and the following noise-assisted training fails even at 5% voltage variation. In Fig. S2 one can see the overlap of some individual temporal curves for initially high and low weight values, which potentially can degrade the memory of an arbitrary SNN. However, increasing the duration of the Hebbian stage of training up to 100 seconds leads to improvement of the results (Fig. 6a).

According to the data obtained, switching voltage variation of 10% is a critical threshold for a given pulse shape in a particular SNN architecture (Fig. 6 b,c). Performance of the noise training is determined mostly by the success of the previous Hebbian training: if the latter works successfully, then the noise-assisted synaptic weight stabilization or their further consolidation, that is depression of small weights and potentiation of high weights, is observed. For the variations of 15% and 25%, in turn, rather unstable Hebbian learning takes place, in which at least half of the experiments performed are unsuccessful, that is the weights with low-rate inputs become higher, and vice versa for the weights of high-rate inputs (see Fig. 6 c,d). Moreover, even at successful first stage, the holding noise-assisted effect is not observed in some cases (weight W2 in Fig. 6 c,d).

As mentioned in the ‘Samples and Methods’ section, modeling of the noise-assisted training with ZrO_2(Y)-based memristors implies varying memristor conductance in high resistive state, ions jump activation energy and switching voltage parameters from cycle to cycle. As mentioned in the ‘Samples and Methods’ section, modeling of the noise-assisted training with ZrO_2(Y)-based memristors implies varying memristor conductance in high

resistive state, ions jump activation energy and switching voltage parameters from cycle to cycle.

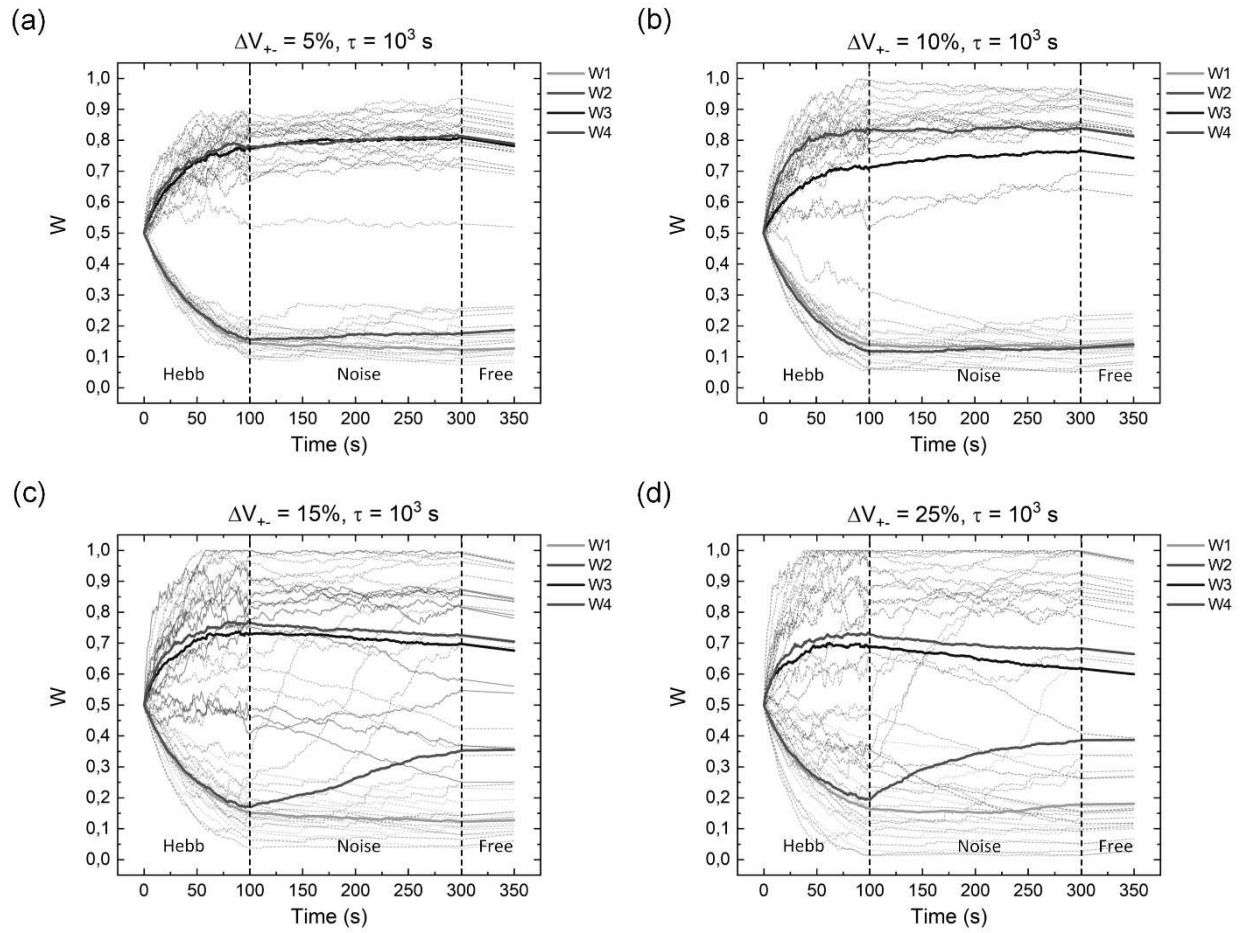

Fig. 6. Temporal trace of conductivity in 4-to-1 SNN simulation with different memristor switching voltage variations (relative standard deviation, ΔV_{+-}): (a) 5%; (b) 10%; (c)15%; (d)25%, at the constant retention time of 10^3 s. All designations and parameters are as in Fig. 5a,c, except the duration of the Hebbian learning, which is 100 s.

As mentioned in the 'Samples and Methods' section, modeling of the noise-assisted training with ZrO_2(Y)-based memristors implies varying memristor conductance in the high resistive state, the activation energy of the ion jumps and the switching voltage parameters from cycle to cycle. The basic values for these parameters were set for the simulation experiments as follows: 10^{-5} S, 0.7 eV, and 2V, for conductance, activation energy, and switching voltage respectively. As the retention time of ZrO_2(Y)-based memristive device is considered infinite, we should talk not about preservation of synaptic weights in SNN, but rather about stabilization of their updates during Hebbian and noise-assisted phases of training.

First of all, we conduct simulation for the case when all parameters are fixed, i.e. excluding their variation. In this situation, the Hebbian learning stage, as well as the noise-assisted stabilization of the ZrO_2(Y)-based memristive weights, is also observed (Fig. 7).

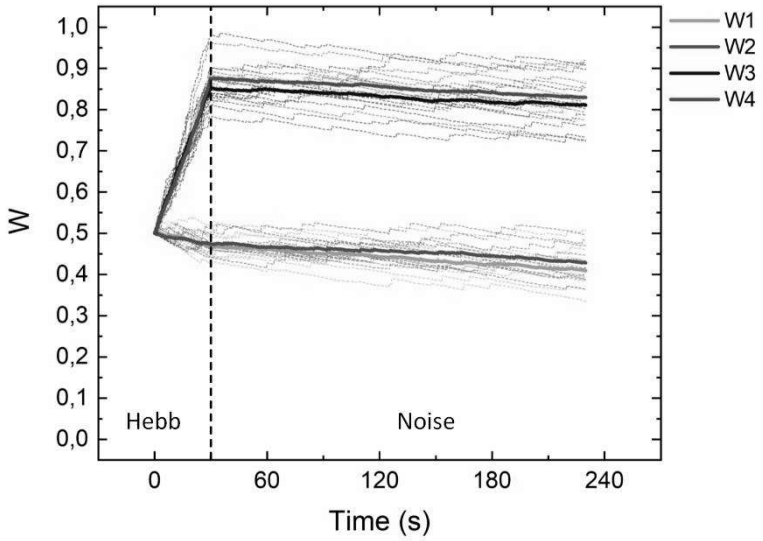

Fig. 7. Simulation results for ZrO_2(Y)-based memristive weights in 4-t-1 SNN without variation of the memristor model parameters. The scheme of experiment: 30 seconds for Hebbian training, and 200 seconds for noise-assisted weight stabilization.

The experiments with variation of the ZrO_2(Y)-based memristor model parameters show that the smallest influence on the weights stabilization effect was made by conductivity variability in high-resistance state (Fig. 8a), while the variation of switching voltages can make significant adjustments to the operation of the SNN (Fig. 8 b-d). It is interesting to note that the combination of the variation effects for all 3 parameters considered makes the resulting temporal dependence of training even more regular than those for the separate sources of variability (compare Fig. 8d with Fig. 8b,c).

It is worth noting that in the case of memristive weights with infinite retention time, as for ZrO_2(Y)-based samples, the above-mentioned regularity became unchanged, that is, if Hebbian training stage is successful, then the noise-assisted stabilization or preservation of weights is successful too. The opposite is not valid, i.e. if Hebbian learning is unsuccessful, then the noise-assisted STDP-based weight updates will not fix this situation, in the sense that the pattern which should be encoded in the SNN's weight array is neither restored nor consolidated.

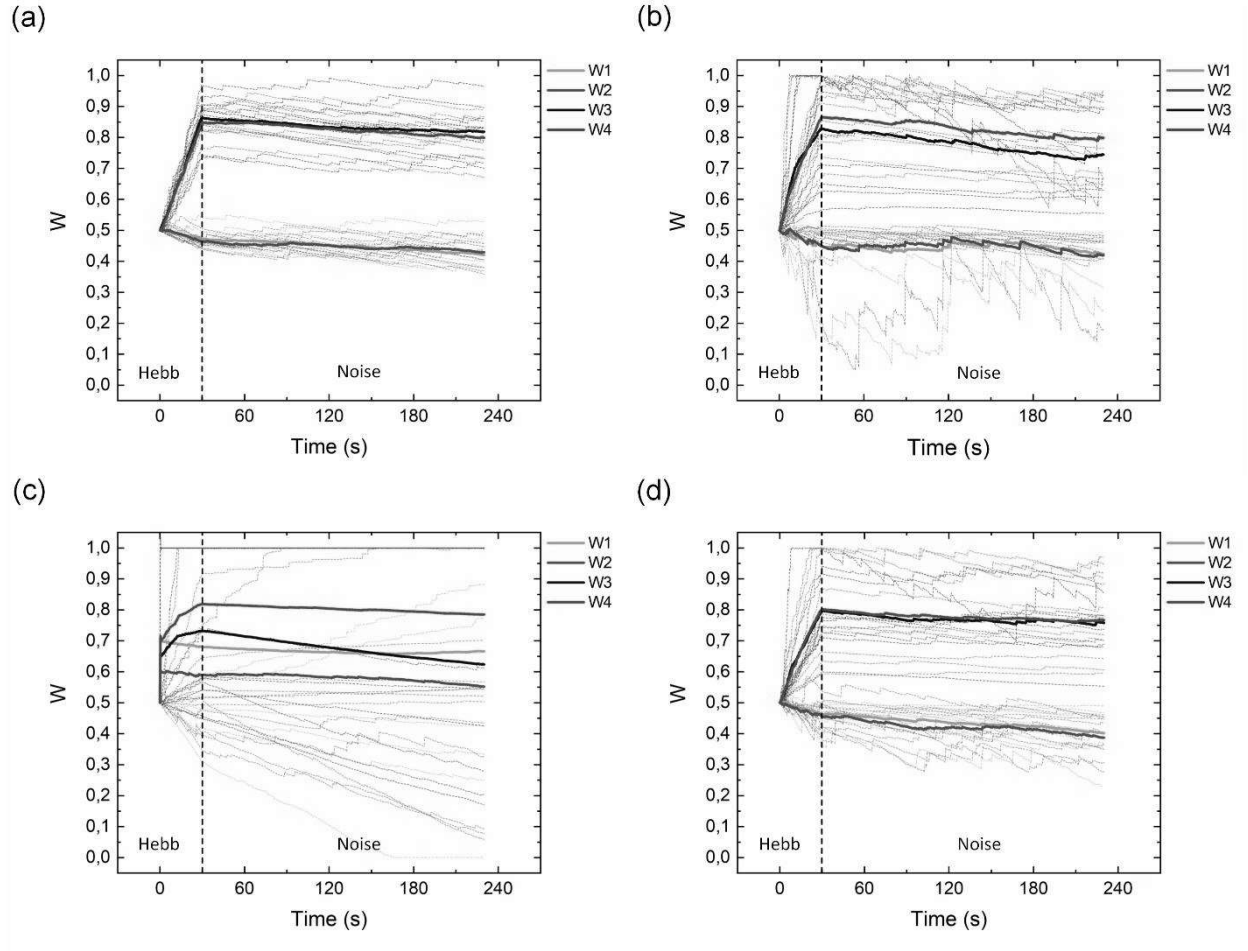

Fig. 8. Simulation results for ZrO_2(Y)-based memristors with parameter variation of: (a) G_{min}, by an order of magnitude (10^{-5} – 10^{-6} S); (b) ion jump activation energy with a SD variation of 10%; (c) both SET and RESET switching voltages with a SD variation of 20%. In (d) the combined effect of the G_{min} conductivity, ion jump activation energy and switching voltages variation is shown. The scheme of the experiment is: 30 seconds for Hebbian training, and 200 seconds for noise-assisted weight stabilization. Fig. S3 a-d describes model *I-V* curves for every experiment, respectively.

Discussion

We have seen that the memory trace, or engram, of the memristive SNN is preserved even if unreliable memristor elements are used — with a finite state retention time, as well as the variable switching voltages. This mechanism is believed to be quite universal, that is, it can emerge in SNNs with different architectures and connection topologies, and can be appropriate for almost arbitrary data domain tasks and sensor modality (video, auditory, tactile, etc.). This assumption may be based on the following qualitative reasoning.

Let's consider the simplest theoretical case of STDP, its additive version based on pairs, which means that only pairs of pre- and postsynaptic spikes give rise to weight updates, the

amplitude of which does not depend on the weight itself but only on the delay time between pre- and post-spikes. Its STDP window is described as follows

$$\Delta w(t) = \begin{cases} A_+ \exp(-t/\tau_+), t \geq 0, \\ A_- \exp(t/\tau_-), t < 0, \end{cases} \quad (1)$$

where A_+, A_- and τ_+, τ_- are amplitudes and characteristic times for the delays of the positive and negative shoulders of the STDP window, respectively, while *t* is a delay between the post- and presynaptic spikes considered. We also consider the nearest-neighbor scheme of pairing events, that is only the nearest spikes of pre-post pairs give rise to synaptic updates. This scheme corresponds to the STDP memristive, in which the voltage spikes have to be overlapped with each other. Then, following [95], we can calculate the positive and negative average weight changes for each presynaptic spike and for totally uncorrelated pre- and postsynaptic Poisson pulse trains, with rates *x* and *y*, correspondingly

$$\Delta w_+ = A_+ \int_0^\infty e^{-t/\tau_+} e^{-xt}\, e^{-yt} y dt = \frac{A_+ y}{x + y + \tau_+^{-1}}, \quad (2a)$$

$$\Delta w_- = A_- \int_{-\infty}^0 e^{t/\tau_-} e^{xt}\, e^{yt} y dt = \frac{A_- y}{x + y + \tau_-^{-1}}. \quad (2b)$$

Then we should take into account some correlations between pre- and post-spikes. As a first approximation, events in which the postsynaptic spike goes immediately after a given presynaptic one on input *i* and causes the synaptic weight to increase by A_+ should be considered. The share δ_i of these events in the flux of post-neuron spikes is of the order of $\delta_i = w_i x_i / \sum w_k x_k$, where summation is implemented over all inputs of a neuron. Higher-order correlations such as the decreasing delay to the next postsynaptic spike due to the contribution of a given presynaptic spike, are not considered in the model. This approximation is effective when individual contributions are not too large, $\delta_i \ll 1$. Hence, the weight-dependent average update, due to correlations, for each presynaptic spike of some input (index i is omitted hereafter) will be given by

$$\Delta w = A_+ \frac{y\delta}{x} + \frac{A_+ y}{x + y + \tau_+^{-1}}(1 - \delta) + \frac{A_- y}{x + y + \tau_-^{-1}}. \quad (3)$$

It is to be noted that in the case of the IF postsynaptic neuron and small rates $y \ll \tau_{ref}^{-1}$ we have that $\sum w_k x_k = Vy$, with τ_{ref} the refractory period of the IF neuron and *V* the proportionality coefficient, which can be considered as a unitless threshold of this neuron. Then, finally, we have

$$\Delta w = \frac{A_+ w}{V} + \frac{A_+ y}{x + y + \tau_+^{-1}}\left(1 - \frac{wx}{Vy}\right) + \frac{A_- y}{x + y + \tau_-^{-1}}. \quad (4)$$

Substituting $y = x\sum w_k /V$ in Eq. (4) and equating it to 0, we can search for the zeros of this expression. The discriminant of the corresponding quadratic equation with respect to x is positive when the product wx is not too large, and $A_+ > |A_-|$, while simultaneously $A_+\tau_+ < |A_-\tau_-|$. The latter are the classic requirements for characteristics of the additive STDP $(A_+, A_-, \tau_+, \tau_-)$ allowing for positive, as well as negative, weight updates during Hebbian learning [94]. Under these conditions the equation Δw = 0 has 2 solutions in terms of x and, therefore, also y, as y ~ x in our approximation. In terms of the postsynaptic rate, one solution is an unstable point, whereas the second, smaller, is a stable point on the rate axis (see Fig. 9). This means that below the stable point the average STDP weight update is positive so that higher weights increase their values and thus contribute to a simultaneous increase in the postsynaptic rate, pushing it towards the stable point. The same is true for the postsynaptic rates just above the stable point, up to reach a situation in which the weights and the postsynaptic rate switch from increase to decrease.

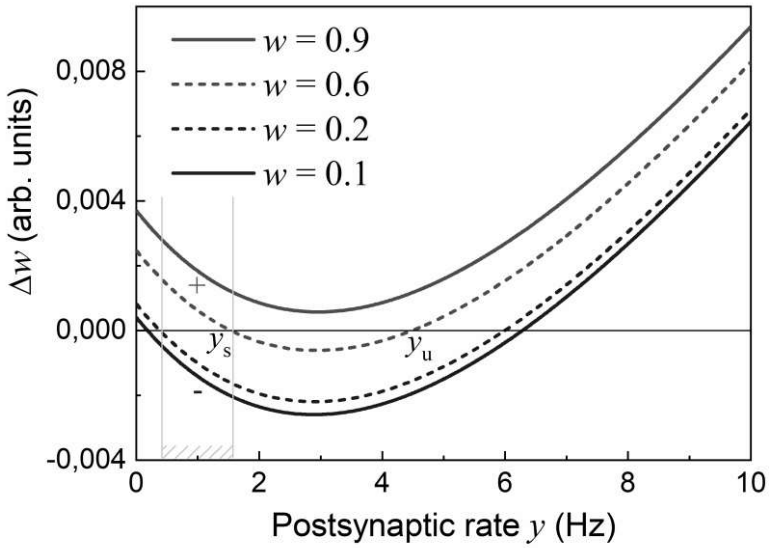

Fig. 9. Spike Rate Dependent Plasticity (SRDP) curves derived from Eq. (4), that is, characteristic dependences of an update of the mean synaptic weight for each presynaptic peak on the postsynaptic Poisson rate y. For our qualitative linear model $y \sim x$, where x is the presynaptic rate; in this specific case we set $y = 0.8x$. Stable and unstable postsynaptic rates for the SRDP curve with w = 0.6 (whereas w_{max} = 1) are indicated by y_s and y_u, respectively. SRDP curves are shown for different weight values. In light grey, the region in which weight updates are non-negative (marked with '+') for all inputs with w≥0.6 and non-positive for w≤0.2 (marked with '-') is highlighted, i.e. weight stabilization and recovering occur in this region for those weight values. The parameters for STDP (A _ +, A _-, τ _ +, τ_-) correspond to those of Fig. S4 and are taken from [95], so these are bio-realistic values. Other parameters are also identical to those of Fig. S4, but here we consider α = γ = 0.

This stable solution is of great interest for our analysis. Indeed, if the Poisson average frequency of the postsynaptic neuron is slightly lower than this point, then for some high values of the weights w_H the expression (4) is positive (or at least non-negative), Δw (w_H) ≥0, while it has opposite sign for small weights, i.e. $\Delta w(w_L) \leq 0$. This is the point where *noise-assisted training* or *weight stabilization* is possible. So, if we apply to the inputs the Poisson pulse trains with the same average frequency, such that it will be slightly less than that corresponding to the stable rate point for some weight demarcation value (i.e. a value such that $w_H > w_D$ and $w_L < w_D$), then the high weights will continue to increase and the low weights to decrease their values or, at least, they will be stabilized (no change will occur).

It is worth noting that expression (4) can be further modified to meet the more realistic conditions of multiplicative-like STDP behavior or weight decrement at each presynaptic event, e.g. as follows

$$\Delta w = \frac{A_+\left(1-\frac{w}{w_{max}}\right)^{\gamma} w}{V} + \frac{A_+\left(1-\frac{w}{w_{max}}\right)^{\gamma} y}{x+y+\tau_+^{-1}}\left(1-\frac{wx}{Vy}\right) + \frac{A_-\left(\frac{w}{w_{max}}\right)^{\gamma} y}{x+y+\tau_-^{-1}} - \alpha\left(\frac{w}{w_{max}}\right)^{\gamma}, \quad (5)$$

where $0 \leq \gamma \leq 1$ is a factor of multiplicativity, α a decrement constant. Despite its greater complexity, expression (5) has similar features as those of expression (4). That is, under some range of parameter values, it has also 2 point solutions in terms of presynaptic rate *x*: one is unstable, the other one is stable, which determines the possibility of *noise-assisted persistence* of SNN's engrams (see Fig. S4 in Supplementary material).

A similar mechanism, that is low-frequency noise retention of synaptic efficiency of interneuronal contacts, could be also be implemented in biological neural networks. As indirect evidence of this we recall: 1) the preservation of memory traces (at least in mammals and humans) even in case of long-term absence of access to these memories [96], despite the limited lifetime of the biomolecular structures (for ion channels — about several hours [97,98]) that maintain synaptic permeability; 2) the presence of so-called pacemaker neurons which influence other neurons by spiking with some fixed rate even in the absence of an external stimulus from the external environment [99]; 3) STDP-like mechanism for changing synaptic weights, which, as noted above, can lead, at least in the case of additive pair-based STDP, to separation (or stabilization) of weights in a low-frequency noise signal.

Therefore, this research also raises a question about the role of noise in the stochastic supra-threshold activity of individual neurons in a biological network of nerve cells, when a memory persistence mechanism is implemented. It is possible to lead experiments with genetic

or biochemical knockout of pacemaker neurons, e.g. in the area of hippocampal structures, to test the above hypothesis. Conducting such an experimental investigation, from our point of view, can be of interest for molecular neuroscientists and memory neurophysiologists.

Conclusions

We have shown that the noise in the form of the low-rate pattern-free train of pulses can have a constructive role in the dynamical maintenance or even fine-tuning of a memory trace stored in a memristive single-layer SNN. The study was carried out by using two different types of oxide-based memristors functioning by microscopically different vacancy drift-determined mechanisms. The principles of the *noise-assisted weight separation* and fine-tuning were qualitatively explained by the model of the pair-based additive STDP rule governing training in a 1-layer SNN with the threshold neurons without a leakage. Although the real memristive STDP behavior is significantly more complex, the basic reasoning in explaining the input noise effect may be the same or similar. Of course, this effect can be treated in any individual layer of arbitrary architecture feed-forward SNN, e.g. there is no direct restriction of the results of the given study to just one layer in SNN architecture. Nevertheless, the case of SNN with some recurrent connections, e.g. with those of lateral inhibition or backward signal propagation, requires an additional investigation. Last but not least, we posed an intriguing question: may such *a noise-assisted mechanism* be realized in a biological nervous system? We also propose one more possible solution to the long-lasting problem of an engram persistence faced with unavoidable turnover of bio-molecules supplying synapse efficacies.

Acknowledgments

Measurements were performed on equipment of the Resource Center for Electrophysical Methods under support of the NBICs Technologies Complex of the National Research Centre “Kurchatov Institute” (#1055). This study was supported by the Government of Russian Federation (project no. 074-02-2018-330(2)) with regard to studying adaptive properties of neurons with memristive weights on noisy signals, Russian Foundation for Basic Research with regard to nanocomposite memristor characterization and STDP learning (project no. 18-29-23041) and with regard to STDP learning of ZrO_2(Y)-based devices (project no. 18-29-23001).

References

[1] Yang Zhang, Zhongrui Wang, Jiadi Zhu, Yuchao Yang, Mingyi Rao, Wenhao Song, Ye Zhuo, Xumeng Zhang, Menglin Cui, Linlin Shen, Ru Huang, and J. Joshua Yang, Appl. Phys. Rev. 7, 011308 (2020); **https://doi.org/10.1063/1.5124027**

[2] Xia, Q., Berggren, K. K., Likharev, K., Strukov, D. B., Jiang, H., Mikolajick, T., ... & Xiong, F. Roadmap on emerging hardware and technology for machine learning. Nanotechnology. (2020). **https://doi.org/10.1088/1361-6528/aba70f**

[3] J. Zhu, T. Zhang, Y. Yang, R. Huang, A comprehensive review on emerging artificial neuromorphic devices, Appl. Phys. Rev. 7, 011312 (2020). **https://doi.org/10.1063/1.5118217**

[4] Alexey Mikhaylov, Alexey Pimashkin, Yana Pigareva, Svetlana Gerasimova, Evgeny Gryaznov, Sergey Shchanikov, Anton Zuev, Max Talanov, Igor Lavrov, Vyacheslav Demin, Victor Erokhin, Sergey Lobov, Irina Mukhina, Victor Kazantsev, Huaqiang Wu and Bernardo Spagnolo, Neurohybrid Memristive CMOS-Integrated Systems for Biosensors and Neuroprosthetics. Frontiers in Neuroscience, 14, 358 (2020). **https://doi.org/10.3389/fnins.2020.00358**

[5] D. Ielmini, Resistive switching memories based on metal oxides: Mechanisms, reliability and scaling. Semicond Sci Technol 31, 1–25 (2016). **https://doi.org/10.1088/0268-1242/31/6/063002.**

[6] E. L. Pankratov and B. Spagnolo, Optimization of impurity profile for p-n junction in heterostructures. Eur. Phys. J. B 46, 15-19 (2005). **https://doi.org/10.1140/epjb/e2005-00233-1**

[7] D. B. Strukov, F. Alibart and R. S. Williams, Thermophoresis/diffusion as a plausible mechanism for unipolar resistive switching in metal–oxide–metal memristors Appl. Phys. A 107, 509–518 (2012). **https://doi.org/10.1007/s00339-012-6902-x**

[8] E. Pérez, D. Maldonado, C. Acal, J. E. Ruiz-Castro, F. J. Alonso, A. M. Aguilera, et al. Analysis of the statistics of device-to-device and cycle-to-cycle variability in TiN/Ti/Al:HfO2/TiN RRAMs. Microelectron Eng 214, 104-109 (2019). **https://doi.org/10.1016/j.mee.2019.05.004**.

[9] J. B. Roldan, D. Maldonado, F. Jimenez-Molinos, C. Acal, J. E. Ruiz-Castro, A. M. Aguilera, et al. Reversible dielectric breakdown in h-BN stacks: a statistical study of the switching voltages. IEEE Int Reliab Phys Symp vol. 2020-April, 1–5 (2020. **https://doi.org/10.1109/IRPS45951.2020.9129147**

[10] Jun Ge, Dongyuan Li, Changqiao Huang, Xuanbo Zhao, Jieli Oin, Huanyu Liu, Weiyong Ye, Wenchao Xu, Zhivu Liu and Shusheng Pan, Memristive synapses with high reproducibility for flexible neuromorphic networks based on biological nanocomposites. Nanoscale 12, 720-730 (2020). **https://doi.org/10.1039/C9NR08001E**

[11] V. Milo, G. Malavena, C. Monzio Compagnoni and D. Ielmini, Memristive and CMOS Devices for Neuromorphic Computing. Materials (Basel, Switzerland) 13, 166 (2020). doi: **10.3390/ma13010166**

[12] M. Prezioso, F. Merrikh-Bayat, B.D. Hoskins, G.C. Adam, K.K. Likharev, D.B. Strukov, Training and operation of an integrated neuromorphic network based on metal-oxide memristors. Nature 521, 61-64 (2015). **https://doi.org/10.1038/nature14441**

[13] A. V. Emelyanov, D. A. Lapkin, V. A. Demin, V. V. Erokhin, S. Battistoni, G. Baldi, A. Dimonte, A. N. Korovin, S. Iannotta, P. K. Kashkarov and M. V. Kovalchuk, AIP Advances 6, 111301-1-9 (2016). **https://doi.org/10.1063/1.4966257**

[14] Peng Yao, Huaqiang Wu, Bin Gao, Sukru Burc Eryilmaz, Xueyao Huang, Wenqiang Zhang, Qingtian Zhang, Ning Deng, Luping Shi, H.-S. Philip Wong & He Qian. Face classification using electronic synapses. Nature communications, 8(1), 1-8. (2017). **https://doi.org/10.1038/ncomms15199**

[15] Can Li, Miao Hu, Yunning Li, Hao Jiang, Ning Ge, Eric Montgomery, Jiaming Zhang, Wenhao Song, Noraica Dávila, Catherine E. Graves, Zhiyong Li, John Paul Strachan, Peng Lin, Zhongrui Wang, Mark Barnell, Qing Wu, R. Stanley Williams, J. Joshua Yang & Qiangfei Xia. Analogue signal and image processing with large memristor crossbars. Nature Electronics, 1(1), 52. (2018). **https://doi.org/10.1038/s41928-017-0002-z**

[16] Mikhaylov AN, Morozov OA, Ovchinnikov PE, Antonov IN, Belov AI, Korolev DS, et al. One-Board Design and Simulation of Double-Layer Perceptron Based on Metal-Oxide Memristive Nanostructures. IEEE Trans Emerg Top Comput Intell 2018;2:371–9. **https://doi.org/10.1109/tetci.2018.2829922**

[17] Zahari, F., Pérez, E., Mahadevaiah, M. K., Kohlstedt, H., Wenger, C., & Ziegler, M. Analogue pattern recognition with stochastic switching binary CMOS-integrated memristive devices. Scientific Reports, 10(1), 1-15. (2020). **https://doi.org/10.1038/s41598-020-71334-x**

[18] C. Li, Z. Wang, M. Rao, D. Belkin, W. Song, H. Jiang, P. Yan, Y. Li, P. Lin, M. Hu, N. Ge, J. P. Strachan, M. Barnell, Q. Wu, R. S. Williams, J. J. Yang, Q. Xia, Long short-term memory networks in memristor crossbar arrays. Nat Mach Intell 1, 49–57 (2019). **https://doi.org/10.1038/s42256-018-0001-4**

[19] Moon, J., Ma, W., Shin, J.H. et al. Temporal data classification and forecasting using a memristor-based reservoir computing system. Nat Electron 2, 480–487 (2019). **https://doi.org/10.1038/s41928-019-0313-3**

[20] Cai, F., Kumar, S., Van Vaerenbergh, T. et al. Power-efficient combinatorial optimization using intrinsic noise in memristor Hopfield neural networks. Nat Electron 3, 409–418 (2020). **https://doi.org/10.1038/s41928-020-0436-6**

[21] Z. Sun, G. Pedretti, E. Ambrosi, A. Bricalli, W. Wang, D. Ielmini, Solving matrix equations in one step with cross-point resistive arrays. Proc. Natl. Acad. Sci., 201815682. (2019). **https://doi.org/10.1073/pnas.1815682116**

[22] Querlioz, D., Bichler, O., Dollfus, P., & Gamrat, C. Immunity to device variations in a spiking neural network with memristive nanodevices. IEEE Transactions on Nanotechnology, 12(3), 288-295. (2013). DOI: 10.1109/TNANO.2013.2250995

[23] Serb, A., Bill, J., Khiat, A. et al. Unsupervised learning in probabilistic neural networks with multi-state metal-oxide memristive synapses. Nat Commun 7, 12611 (2016). **https://doi.org/10.1038/ncomms12611**

[24] E. Covi, R. George, J. Frascaroli, S. Brivio, C. Mayr, H. Mostafa, G. Indiveri, S. Spiga, Spike-driven threshold-based learning with memristive synapses and neuromorphic silicon neurons, J. Phys. D. Appl. Phys. 2018, 51, 34003. **https://doi.org/10.1088/1361-6463/aad361**

[25] Z. Wang, S. Joshi, S. Savel'ev, W. Song, R. Midya, Y. Li, M. Rao, P. Yan, S. Asapu, Y. Zhuo, H. Jiang, P. Lin, C. Li, J. H. Yoon, N. K. Upadhyay, J. Zhang, M. Hu, J. P. Strachan, M. Barnell, Q. Wu, H. Wu, R. S. Williams, Q. Xia, J. J. Yang, Fully memristive neural networks for pattern classification with unsupervised learning. Nat Electron 1, 137–145 (2018). **https://doi.org/10.1038/s41928-018-0023-2**

[26] M. Prezioso, M. R. Mahmoodi, F. Merrikh-Bayat, H. Nili, H. Kim, A. F. Vincent, D. B. Strukov, Spike-timing-dependent plasticity learning of coincidence detection with passively integrated memristive circuits. Nat Commun 9, 5311 (2018). **https://doi.org/10.1038/s41467-018-07757-y**

[27] K. E. Nikiruy, A. V. Emelyanov, V. V. Rylkov, A. V. Sitnikov, V. A. Demin, Adaptive Properties of Spiking Neuromorphic Networks with Synapses Based on Memristive Elements. Tech. Phys. Lett. 45, 386–390 (2019). **https://doi.org/10.1134/S1063785019040278**

[28] S. Brivio, D. Conti, M. V. Nair, J. Frascaroli, E. Covi, C. Ricciardi, G. Indiveri, S. Spiga, Extended memory lifetime in spiking neural networks employing memristive

synapses with nonlinear conductance dynamics. Nanotechnology 2019, 30, 015102. **https://doi.org/10.1088/1361-6528/aae81c**

[29] Prezioso, M., Merrikh Bayat, F., Hoskins, B. et al. Self-Adaptive Spike-Time-Dependent Plasticity of Metal-Oxide Memristors. Sci Rep 6, 21331 (2016). **https://doi.org/10.1038/srep21331**

[30] A.V. Emelyanov, K.E. Nikiruy, V.A. Demin, V.V. Rylkov, A.I. Belov, D.S. Korolev, E.G. Gryaznov, D.A. Pavlov, O.N. Gorshkov, A.N. Mikhaylov and P. Dimitrakis. Yttria-stabilized zirconia cross-point memristive devices for neuromorphic applications. Microelectronic Engineering, 215, 110988. (2019). **https://doi.org/10.1016/j.mee.2019.110988**

[31] Nikita V Prudnikov, Dmitry A Lapkin, Andrey V Emelyanov, Anton A Minnekhanov, Yulia N Malakhova, Sergey N Chvalun, Vyacheslav A Demin and Victor V Erokhin, "Associative STDP-like learning of neuromorphic circuits based on polyaniline memristive microdevices", J. Phys. D: Appl. Phys. 53 414001. (2020) **https://doi.org/10.1088/1361-6463/ab9262**

[32] Minnekhanov, A.A., Emelyanov, A.V., Lapkin, D.A. et al. Parylene Based Memristive Devices with Multilevel Resistive Switching for Neuromorphic Applications. Sci Rep 9, 10800 (2019). **https://doi.org/10.1038/s41598-019-47263-9**

[33] Ryu, J. H., & Kim, S. Artificial synaptic characteristics of TiO_2/HfO_2 memristor with self-rectifying switching for brain-inspired computing. Chaos, Solitons & Fractals, 140, 110236. (2020). **https://doi.org/10.1016/j.chaos.2020.110236**

[34] Kim S, Chen J, Chen YC, Kim MH, Kim H, Kwon MW, et al. Neuronal dynamics in HfOx/AlOy-based homeothermic synaptic memristors with low-power and homogeneous resistive switching. Nanoscale 2019; 11 : 237–45. **https://doi.org/10.1039/c8nr06694a**

[35] A V Emelyanov, K E Nikiruy, A V Serenko, A V Sitnikov, M Yu Presnyakov, R B Rybka, A G Sboev, V V Rylkov, P K Kashkarov, M V Kovalchuk and V A Demin, Self-adaptive STDP-based learning of a spiking neuron with nanocomposite memristive weights, Nanotechnology 31, 045201 (2020) **https://doi.org/10.1088/1361-6528/ab4a6d**

[36] Xia, Q., Yang, J.J. Memristive crossbar arrays for brain-inspired computing. Nat. Mater. 18, 309–323 (2019). **https://doi.org/10.1038/s41563-019-0291-x**

[37] S. Brivio, J. Frascaroli, E. Covi, et al. Stimulated Ionic Telegraph Noise in Filamentary Memristive Devices. Sci Rep 9, 6310 (2019). **https://doi.org/10.1038/s41598-019-41497-3**

[38] D. O. Filatov, D. V. Vrzheshch, O. V. Tabakov, A. S. Novikov, A. I. Belov, I. N. Antonov, et al. Noise-induced resistive switching in a memristor based on ZrO2(Y)/Ta2O5 stack. J Stat Mech Theory Exp 2019;2019:124026. **https://doi.org/10.1088/1742-5468/ab5704**

[39] Agudov N V., Safonov A V., Krichigin A V., Kharcheva AA, Dubkov AA, Valenti D, Guseinov DV, Belov AI, Mikhaylov AN, Carollo A, Spagnolo B. Nonstationary distributions and relaxation times in a stochastic model of memristor. J Stat Mech Theory Exp 2020;2020:024003. **https://doi.org/10.1088/1742-5468/ab684a**

[40] Fatt, P., Katz, B. "Spontaneous subthreshold activity at motor nerve endings". J Physiol. 117 (1): 109–128. (1952). **https://doi:10.1113/jphysiol.1952.sp004735**

[41] Lauger, P. "Current noise generated by electrogenic ion pumps". Eur Biophys J. 11 (2): 117–128. (1984).

[42] R. Brunetti, F. Affinito, C. Jacoboni, E. Piccinini & M. Rudan "Shot noise in single open ion channels: A computational approach based on atomistic simulations". Journal of Computational Electronics. 6 (1): 391–394. (2007). **https://doi:10.1007/s10825-006-0140-4**

[43] Spagnolo B, Valenti D, Guarcello C, Carollo A, Persano Adorno D, Spezia S, Pizzolato N, Di Paola B. Noise-induced effects in nonlinear relaxation of condensed matter systems. Chaos, Solitons & Fractals 2015;81:412-424. **https://doi.org/10.1016/j.chaos.2015.07.023**

[44] Spagnolo B, Guarcello C, Magazzù L, Carollo A, Persano Adorno D, Valenti D. Nonlinear Relaxation Phenomena in Metastable Condensed Matter Systems. Entropy 2017;19:20. **https://doi.org/10.3390/e19010020**

[45] Valenti D, Magazzù L, Caldara P, Spagnolo B. Stabilization of quantum metastable states by dissipation. Phys Rev B **2015; 91:**235412. **https://doi.org/10.1103/PhysRevB.91.235412**

[46] Dubkov AA, Spagnolo B. Verhulst model with Lévy noise excitation. Eur. Phys. J. B 2008; 65: 361–367. **https://doi.org/10.1140/epjb/e2008-00337-0**

[47] Falci G, La Cognata A, Berritta M, D'Arrigo A, Paladino E, Spagnolo B. Design of a Lambda system for population transfer in superconducting nanocircuits. Phys. Rev. B 2013;**87**:214515. **https://doi.org/10.1103/PhysRevB.87.214515**

[48] Spagnolo B, Valenti D. Volatility Effects on the Escape Time in Financial Market Models. Int J Bifurc Chaos 2008;18:2775 – 2786. **https://doi.org/10.1142/S0218127408022007**

[49] Yu. V. Ushakov, A. A. Dubkov, and B. Spagnolo, "*Spike train statistics for consonant and dissonant musical accords in a simple auditory sensory model*", Phys. Rev. E **81**, 041911 (2010). **https://doi.org/10.1103/PhysRevE.81.041911**

[50] Yu.V. Ushakov, A.A. Dubkov and B. Spagnolo, "*Regularity of spike trains and harmony perception in a model of the auditory system*", Physical Review Letters **107**, 108103 (2011). **https://doi.org/10.1103/PhysRevLett.107.108103**

[51] Giuffrida A, Valenti D, Ziino G, Spagnolo B, Panebianco A. A stochastic interspecific competition model to predict the behaviour of Listeria monocytogenes in the fermentation process of a traditional Sicilian salami. European Food Research and Technology 2009;228:767-775. **https://doi.org/10.1007/s00217-008-0988-6**

[52] Alexander A. Dubkov and Bernardo Spagnolo, Acceleration of Diffusion in Randomly Switching Potential with Supersymmetry, Phys. Rev. E **72**, 041104 (2005). **https://doi.org/10.1103/PhysRevE.72.041104**

[53] Denaro G, Valenti D, La Cognata A, Spagnolo B, Bonanno A, Basilone W, Mazzola S, Zgozi S, Aronica S. Spatio-temporal behaviour of the deep chlorophyll maximum in Mediterranean Sea: Development of a stochastic model for picophytoplankton dynamics. Ecological Complexity 2013; **13:** 21-34. **http://dx.doi.org/10.1016/j.ecocom.2012.10.002**

[54] McNamara B, Wiesenfeld K, Roy R. Phys Rev Lett 1988;60:2626-2629. **https://doi.org/10.1103/PhysRevLett.60.2626**

[55] Mantegna RN, Spagnolo B, Stochastic Resonance in a Tunnel Diode in the Presence of White or Colored Noise. Nuovo Cimento D 1995;**17:**873-881. **https://doi.org/10.1007/BF02451845**

[56] Lanzara E, Mantegna RN, Spagnolo B, Zangara R. Experimental study of a nonlinear system in the presence of noise: The stochastic resonance. Am J Phys 1997;65:341–9. **https://doi.org/10.1119/1.18520.**

[57] Gammaitoni L, Hänggi P, Jung P, Marchesoni F. Stochastic resonance. Rev Mod Phys 1998;70:223–87. **https://doi.org/10.1103/RevModPhys.70.223**.

[58] Mantegna RN, Spagnolo B, Trapanese M. Linear and Nonlinear Experimental Regimes of Stochastic Resonance. Phys Rev E 2001;63: 011101. **https://doi.org/10.1103/PhysRevE.63.011101**

[59] R. N. Mantegna and B. Spagnolo, Probability distribution of the Residence Times in Periodically Fluctuating Metastable Systems, Int. J. of Bifurcation and Chaos, Vol. **8**, 783-790 (1998). **https://doi.org/10.1142/S0218127498000577**

[60] Hurtado P I, Marro J and Garrido P, Metastability, nucleation, and noise-enhanced stabilization out of equilibrium. Phys. Rev. E 74 050101 (2006) **https://doi.org/10.1103/PhysRevE.74.050101**

[61] A. L. Pankratov and B. Spagnolo, "*Suppression of Timing Errors in Short Overdamped Josephson Junctions*", Phys. Rev. Lett. **93**, 177001 (2004). **https://doi.org/10.1103/PhysRevLett.93.177001**

[62] Jing-hui Li and Jerzy Łuczka, Thermal-inertial ratchet effects: Negative mobility, resonant activation, noise-enhanced stability, and noise-weakened stability. Phys. Rev. E 82, 041104 (2010). **https://doi.org/10.1103/PhysRevE.82.041104**

[63] Spagnolo B, Dubkov AA, Pankratov AL, Pankratova EV, Fiasconaro A, Ochab–Marcinek A. Lifetime of metastable states and suppression of noise in Interdisciplinary Physical Models. Acta Phys Pol B 2007;38:1925-1950.

[64] Spagnolo B, Dubkov AA, Agudov NV. Enhancement of stability in randomly switching potential with metastable state. The European Physical Journal B 2004;40: 273-281. **https://doi.org/10.1140/epjb/e2004-00268-8**

[65] Doering CR, Gadoua JC. Resonant activation over a fluctuating barrier. Phys Rev Lett 1992;69:2318–21. **https://doi.org/10.1103/PhysRevLett.69.2318**.

[66] Pizzolato N, Fiasconaro A, Persano Adorno D, Spagnolo B. Resonant activation in polymer translocation: new insights into the escape dynamics of molecules driven by an oscillating field. Physical Biology 2010;7**:** 034001. **https://doi.org/10.1088/1478-3975/7/3/034001**

[67] Guarcello C**,** Valenti D**,** Carollo A**,** Spagnolo B. Effects of Lévy noise on the dynamics of sine-Gordon solitons in long Josephson junctions. Journal of Statistical Mechanics: Theory and Experiment 2016; 2016:054012. **https://doi.org/10.1088/1742-5468/2016/05/054012**

[68] Bart Kosko, Sanya Mitaim, Stochastic resonance in noisy threshold neurons. Neural Networks, V. 16, Issues 5–6, P 755-761 (2003).

[69] Javier G. Orlandi, Jordi Soriano, Enrique Alvarez-Lacalle, Sara Teller, Jaume Casademunt, Noise focusing and the emergence of coherent activity in neuronal cultures. Nature Phys 9, 582–590 (2013). **https://doi.org/10.1038/nphys2686**

[70] Li C, Chen L, Aihara K, Transient Resetting: A Novel Mechanism for Synchrony and Its Biological Examples. PLOS Computational Biology 2(8): e103. (2006) **https://doi.org/10.1371/journal.pcbi.0020103**

[71] Srivastava, Nitish; C. Geoffrey Hinton; Alex Krizhevsky; Ilya Sutskever; Ruslan Salakhutdinov "Dropout: A Simple Way to Prevent Neural Networks from overfitting" Journal of Machine Learning Research. 15 (1): 1929–1958 (2014).

[72] S.A. Lobov, M.O. Zhuravlev, V.A. Makarov, V.B. Kazantsev, Noise Enhanced Signaling in STDP Driven Spiking-Neuron Network. Math. Model. Nat. Phenom. Vol. 12, No. 4, pp. 108-123 (2017). **https://doi.org/10.1051/mmnp/201712409**

[73] Elvira Juzekaeva, Azat Nasretdinov, Silvia Battistoni, Tatiana Berzina, Salvatore Iannotta, Rustem Khazipov, Victor Erokhin, Marat Mukhtarov. Coupling cortical neurons through electronic memristive synapse. Adv. Mater. Technol. 4, 1800350 (2019). **https://doi.org/10.1002/admt.201800350**

[74] F. Merrikh Bayat, M. Prezioso, B. Chakrabarti, I. Kataeva, D. B. Strukov. 2016. Advancing Memristive Analog Neuromorphic Networks: Increasing Complexity, and Coping with Imperfect Hardware Components. arXiv:1611.04465

[75] Querlioz D, Bichler O, Dollfus P, Gamrat C. 2013. Immunity to device variations in a spiking neural network with memristive nanodevices. IEEE Trans Nanotechnol 12(3):288–295

[76] Sboev A., Serenko A., Rybka R., and Vlasov D. 2020. Solving a classification task by spiking neural network with STDP based on rate and temporal input encoding. Math Meth Appl Sci. 43: 7802–7814

[77] Wenqiang Zhang, Bin Gao, Jianshi Tang, Peng Yao, Shimeng Yu, Meng-Fan Chang, Hoi-Jun Yoo, He Qian and Huaqiang Wu. 2020. Neuro-inspired computing chips. Nature Electronics 3: 371–382.

[78] M.N. Martyshov, A.V. Emelyanov, V.A. Demin, K.E. Nikiruy, A.A. Minnekhanov, S.N. Nikolaev, A.N. Taldenkov, A.V. Ovcharov, M. Yu. Presnyakov, A.V. Sitnikov, A.L. Vasiliev, P.A. Forsh, A.B. Granovsky, P.K. Kashkarov, M.V. Kovalchuk, and V.V. Rylkov. Multifilamentary Character of Anticorrelated Capacitive and Resistive Switching in Memristive Structures Based on (Co−Fe−B)x(LiNbO3)100−x Nanocomposite. Phys. Rev. Applied 14, 034016. 2020. **https://doi.org/10.1103/PhysRevApplied.14.034016**

[79] Alexey Mikhaylov, Alexey Belov, Dmitry Korolev, Ivan Antonov, Valentina Kotomina, Alina Kotina, Evgeny Gryaznov, Alexander Sharapov, Maria Koryazhkina, Ruslan Kryukov, Sergey Zubkov, Artem Sushkov, Dmitry Pavlov, Stanislav Tikhov, Oleg Morozov, David Tetelbaum. Multilayer Metal-Oxide Memristive Device with Stabilized Resistive Switching. Adv. Mater. Technol., 5, 1900607 (2020) **https://doi.org/10.1002/admt.201900607**

[80] D. Filatov, S. Tikhov, O. Gorshkov, I. Antonov, M. Koryazhkina, A. Morozov. Ion migration polarization in the yttria stabilized zirconia based metal-oxide-metal and metal-oxide-semiconductor stacks for resistive memory. Advances in Condensed Matter Physics. – 2018. – Vol.2018. – P.2028491. **https://doi.org/10.1155/2018/2028491**

[81] Measurement of the activation energies of oxygen ion diffusion in yttria stabilized zirconia by flicker noise spectroscopy / Arkady V. Yakimov, Dmitry O. Filatov, Oleg N. Gorshkov, Dmitry A. Antonov, Dmitry A. Liskin, Ivan N. Antonov, Alexander V. Belyakov, Alexey V. Klyuev, Angelo Carollo, Bernardo Spagnolo // Applied Physics Letters. – 2019. – Vol.114. – P.253506. **https://doi.org/10.1063/1.5098066**

[82] A Memristor with Low Switching Current and Voltage for 1S1R Integration and Array Operation / N.K. Upadhyay, W. Sun, P. Lin, S. Joshi, R. Midya, X. Zhang, Z. Wang, H. Jiang, J.H. Yoon, M. Rao, M. Chi, Q. Xia, J.J. Yang // Adv. Electron. Mater. – 2020. – Vol. 6, No. 5. – P. 1901411. **https://doi.org/10.1002/aelm.201901411**

[83] Nikiruy, K.E., Emelyanov, A.V., Demin, V.A. et al. A Precise Algorithm of Memristor Switching to a State with Preset Resistance. Tech. Phys. Lett. 44, 416–419 (2018). **https://doi.org/10.1134/S106378501805022X**

[84] Kristina E. Nikiruy, Igor A. Surazhevsky, Vyacheslav A. Demin, and Andrey V. Emelyanov, «Spike-Timing-Dependent and Spike-Shape-Independent Plasticities with Dopamine-Like Modulation in Nanocomposite Memristive Synapses». Phys. Status Solidi A 2020, 1900938, **https://doi.org/10.1002/pssa.201900938**

[85] Xiaojian Zhu, Qiwen Wang & Wei D. Lu, Memristor networks for real-time neural activity analysis. Nature Coomunications 11, 2439 (2020). **https://doi.org/10.1038/s41467-020-16261-1**

[86] S. Kvatinsky et al., "VTEAM – A General Model for Voltage Controlled Memristors," IEEE Transactions On Circuits And Systems—Ii: Express Briefs, Vol. 62, No. 8, August 2015.].

[87] I. Surazhevsky et al., «Software and hardware implementations of the spike and formal neural networks main components», №96, Nanoindustry, 2020

[88] Gerasimova, S.A. & Mikhaylov, Alexey & Belov, A. & Korolev, Dmitry & Guseinov, Davud & Lebedeva, Albina & Gorshkov, O.N. & Kazantsev, Victor. (2018). Design of memristive interface between electronic neurons. AIP Conference Proceedings. 1959. 090005. **https://doi.org/10.1063/1.5034744**

[89] K. E. Nikiruy, A. V. Emelyanov, V. A. Demin, A. V. Sitnikov, A. A. Minnekhanov, V. V. Rylkov, P. K. Kashkarov, and M. V. Kovalchuk, «Dopamine-like STDP modulation in nanocomposite memristors» AIP Advances 9, 065116 (2019).

[90] A. N. Matsukatova, K. E. Nikiruy, A. A. Minnekhanov, S. N. Nikolaev, A. V. Emelyanov, V. A. Levanov, K. Yu. Chernoglazov, A. V. Sitnikov, A. S. Vedeneev, A. S. Bugaev & V. V. Rylkov. Resistive Switching of Memristors Based on $(Co_{40}Fe_{40}B_{20})_x(LiNbO_3)_{100-x}$ Nanocomposite with a $LiNbO_3$ Interlayer: Plasticity and Time Characteristics. J. Commun. Technol. Electron. 65, 1198–1203 (2020). **https://doi.org/10.1134/S1064226920090077**

[91] V.V. Rylkov, S.N. Nikolaev, V.A. Demin, A. V. Emelyanov, A. V. Sitnikov, K. E. Nikiruy, V. A. Levanov, M. Yu. Presnyakov, A. N. Taldenkov, A. L. Vasiliev, K. Yu. Chernoglazov, A. S. Vedeneev, Yu. E. Kalinin, A. B. Granovskii, V. V. Tugushev, and A. S. Bugaev. Transport, Magnetic, and Memristive Properties of a Nanogranular (CoFeB)x(LiNbOy)100–x Composite Material, J. Exp. Theor. Phys. 126, 353 (2018).

[92] Rylkov, V.V., Emelyanov, A.V., Nikolaev, S.N., K. E. Nikiruy, A. V. Sitnikov, E. A. Fadeev, V. A. Demin & A. B. Granovsky, Transport Properties of Magnetic Nanogranular Composites with Dispersed Ions in an Insulating Matrix. J. Exp. Theor. Phys. 131, 160–176 (2020). **https://doi.org/10.1134/S1063776120070109**

[93] Guseinov, Davud & Tetelbaum, D. & Mikhaylov, Alexey & Belov, A & Shenina, M & Korolev, Dmitry & Antonov, I & Kasatkin, A & Gorshkov, O.N. & Okulich, E. & Okulich, V & Bobrov, A. & Malekhonova, N. & Pavlov, Dmitri & Gryaznov, E & Gryaznov, Evgeny. (2017). Filamentary model of bipolar resistive switching in capacitor-like memristive nanostructures on the basis of yttria-stabilised zirconia. International Journal of Nanotechnology. 14. 604-617. **https://doi.org/10.1504/IJNT.2017.083436**

[94] A.N. Mikhaylov, E.G. Gryaznov, A.I. Belov, D.S. Korolev, A.N. Sharapov, D.V. Guseinov, D.I. Tetelbaum, S.V. Tikhov, N.V. Malekhonova, A.I. Bobrov, D.A. Pavlov, S.A. Gerasimova, V.B. Kazantsev, N.V. Agudov, A.A. Dubkov, C.M.M. Rosário, N.A. Sobolev, B. Spagnolo. Field- and irradiation-induced phenomena in memristive nanomaterials. Physica Status Solidi C. – 2016. – Vol.13. – P.870-881.

[95] Izhikevich, E. M., & Desai, N. S. Relating STDP to BCM. Neural Computation, 15(7), 1511–1523 (2003). **https://doi.org/10.1162/089976603321891783**

[96] Vorob'eva, N.S., Ivashkina, O.I., Toropova, K.A. et al. Long-Term Contextual Memory in Mice: Persistence and Associability with Reinforcement. Neurosci Behav Physi 47, 780–786 (2017). **https://doi.org/10.1007/s11055-017-0467-2**

[97] Erik D. Roberson and J. David Sweatt. 1999. A Biochemical Blueprint for Long-Term Memory. Learning & Memory 6:381–388

[98] Paul Smolen, Douglas A. Baxter, and John H. Byrne. 2019. Learning & Memory 26:133–150

[99] Jan-Marino Ramirez, Andrew K Tryba and Fernando Peňa. 2004. Pacemaker neurons and neuronal networks: an integrative view. Current Opinion in Neurobiology, 14:665–674

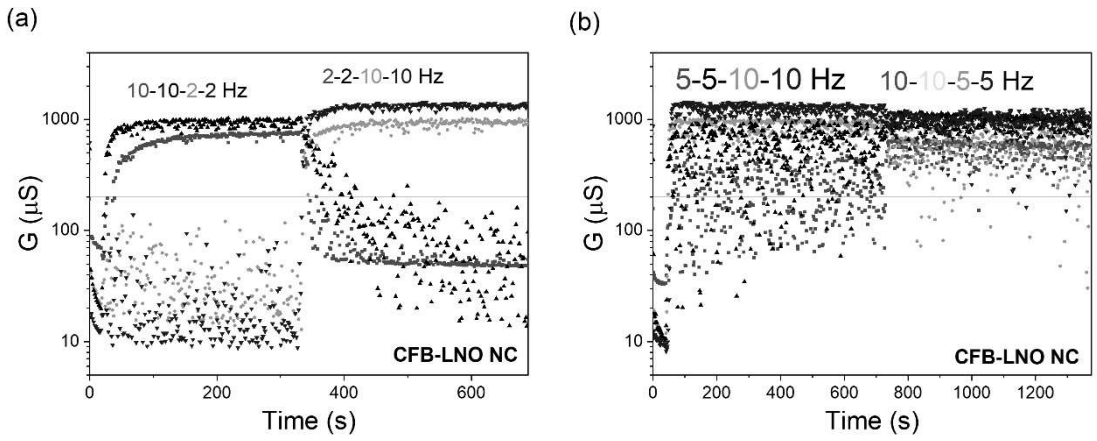

Fig. S1. Temporal dependence of conductivity of memristors in 4-in-1 neural network with same as in (Fig. 5a) pre- and postspikes parameters, but different prespikes ratio – a) 10 Hz : 2 Hz, b) 10 Hz : 5 Hz. Graphs show that possibility of Hebbian learning a) remains for some ratio less than in Fig. 5 – 5 : 1, and b) lack of such learning for lesser ratio – 2 : 1.

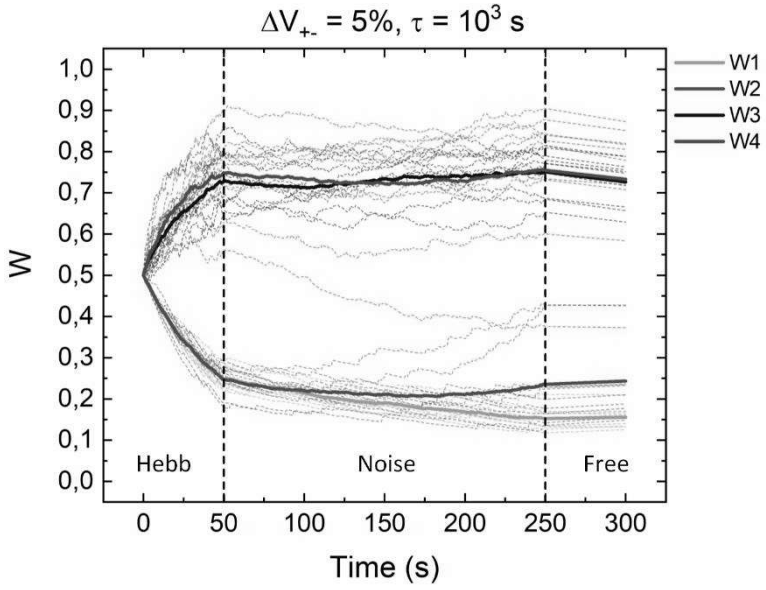

Fig. S2. Statistical temporal dependence of conductivity in 4-to-1 neural network CAD modeling with a 5% memristor's switching voltage variation at constant retention time which equals 10^3 seconds. All graphs represent dynamics (with highlighted trends averaged after 10 runs) of four synaptic weights with different input average frequencies for the first 50 seconds: 1Hz for W1 and W2, 10Hz for W3 and W4; then noise-assisted learning with frequency 1Hz for all inputs during 200 seconds, and relaxation process for 50 seconds

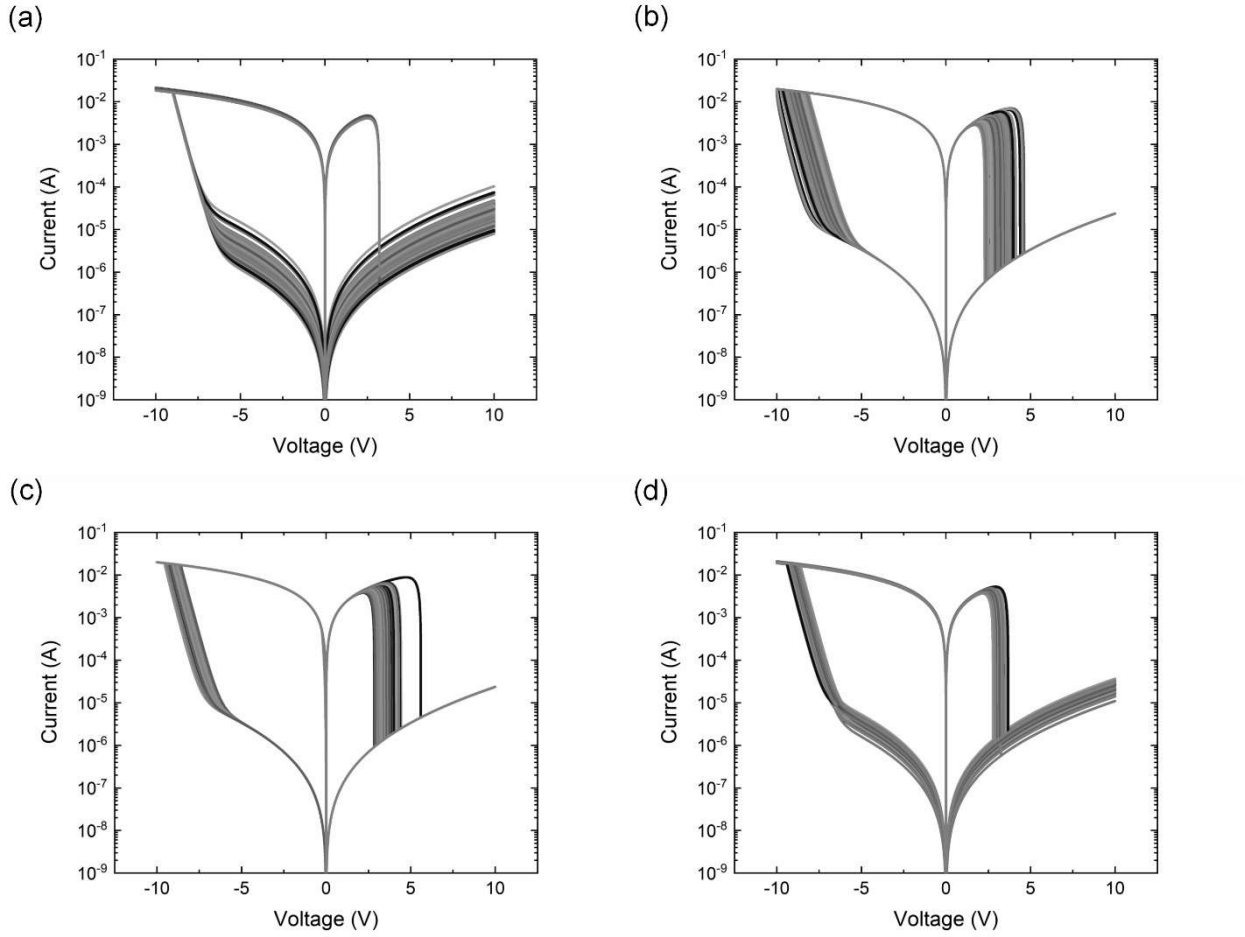

Fig. S3. Model *IV-curve* for ZrO_2(Y)-based memristors with parameter variations: a) G_{min} by an order of magnitude (10^{-5} – 10^{-6} S); b) 10% ion jump activation energy variation; C) 20% switching voltages variation; d) the combined effect of the G_{min} conductivity, ion jump activation energy and switching voltages variations.

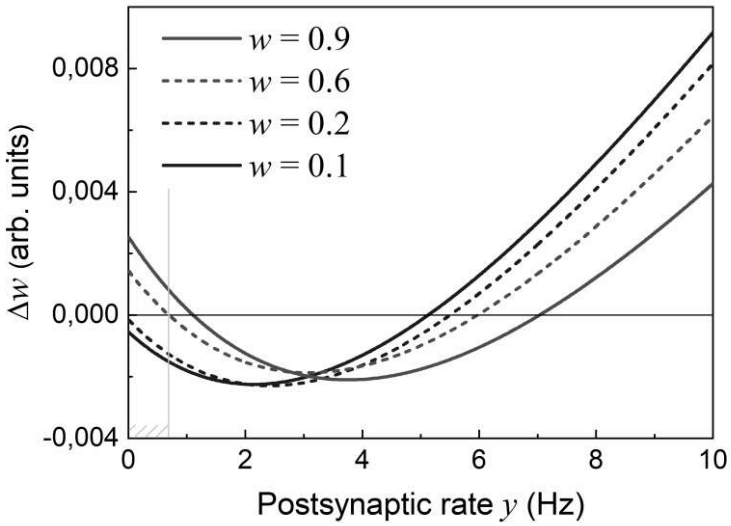

Fig. S4. Spike Rate Dependent Plasticity (SRDP) curves for the case of an average weight update described by formula (5) in the main text, with parameters: $A_+ = 1.03$, $A_- = -0.51$, $\tau_+ = 34$ ms, $\tau_- =$

14 ms, $\gamma = 0.02$, $V = 250$, $\alpha = 0.001$, $y = 0.8x$. SRDP curves are shown for different weight values (whereas $w_{max} = 1$). In light grey, there is highlighted the region where the weight updates are positive for all inputs with $w > 0.6$ and negative for $w < 0.2$, i.e. the weight stabilization and recovering take place in this region for those weight values.